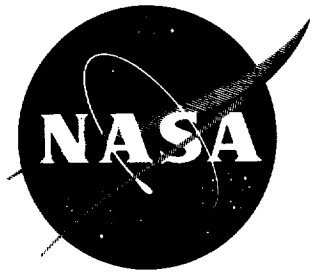

TECHNICAL NOTE

D-1424

RADIATIVE HEAT TRANSFER AND ABSORPTION BEHIND

A HYPERSONIC NORMAL SHOCK WAVE

By Kenneth K. Yoshikawa and Dean R. Chapman

Ames Research Center
Moffett Field, Calif.

NATIONAL AERONAUTICS AND SPACE ADMINISTRATION

WASHINGTON September 1962

NATIONAL AERONAUTICS AND SPACE ADMINISTRATION

TECHNICAL NOTE D-1424

RADIATIVE HEAT TRANSFER AND ABSORPTION BEHIND A HYPERSONIC NORMAL SHOCK WAVE

By Kenneth K. Yoshikawa and Dean R. Chapman

SUMMARY

A study is made of the emission, absorption, and decay of radiant energy by high-temperature air behind a one-dimensional shock wave in hypersonic flow. The analysis is developed for the case of gray radiation in local thermodynamic equilibrium. A relatively simple solution of the integro-differential equations has been obtained for the magnitude of the radiant fluxes in the upstream and downstream directions. In this solution, the temperature distribution is not computed initially, but is computed subsequent to the determination of the optical thickness. Numerical results are presented for the distribution of upstream and downstream radiation heat flux for pressures between 1 and 10^3 atmospheres, and for temperatures between 10,000° K and 15,000° K. The flight conditions are outlined under which the decay and absorption of radiant energy become important in the gas cap of an entry vehicle.

INTRODUCTION

The study of heat transfer by radiation in a gaseous media is of considerable interest in various scientific problems, and of particular concern to the heat protection of space vehicles during atmosphere entry at velocities above the escape velocity for the earth (refs. 1-6). At these high velocities, and at the modestly high densities encountered behind strong shock waves, the absorption as well as emission of radiant energy by the shock layer can be a significant part of the energy crossing the shock wave. For such conditions the influence of absorption must be included in an analysis of this problem (refs. 7, 8). A general formulation of the equations for heat transfer by radiation and absorption has been presented by Goulard (ref. 9). The fundamentals of the basic transfer theory behind their formulation may be found in various books on astrophysics (e.g., refs. 10, 11). A number of papers have been published in which calculations of the radiative heat transfer from the hot-gas cap to a reentry vehicle are made under the simplifying assumptions of constant temperature and negligible effects of radiation absorption (refs. 1, 2, 3). Recently, a very general form of the basic radiation equations has been presented by Viskanta (ref. 7).

In the present report, the radiation heat flux behind strong normal shock waves wherein radiation absorption and decay of radiation emission are important has been calculated under the following assumptions:

1. Gray radiation with local thermodynamic equilibrium of the radiation and the gas properties behind the shock wave.

2. Negligible absorption upstream of the shock wave of the radiation from the region downstream of the shock wave.

3. Transparent shock front (zero reflection of radiation passing upstream through shock).

4. Black body wall at a temperature very small compared to the gas temperature.

5. Negligible heat transfer by thermal conduction and convection compared to radiation.

6. Radiant heat flux at the wall in a real flow with shock detachment distance, L, is the same as that in an idealized one-dimensional hypersonic flow wherein all downstream radiation is absorbed at a distance L downstream of the shock wave.

NOTATION

The notation adopted is that of Goulard (ref. 9).

A, B, B_0, B_1, C, D, f	constants in equation (A5)
a, b, c	constants in equation (A2)
a_n	coefficient of expansion in equation (A1)
B_ν	Planck's function (eq. (2c))
c	velocity of light
c_p	specific heat at constant pressure
d	constant in equation (21)
$E_n(t)$, $E_i(t)$	exponential integral (eq. (2a))
E_t	radiation intensity, $4\bar{\mu}\sigma T^4$
F, F_0, F_1, F_2, F_t, F_s, F_w	dimensionless flux functions (eqs. (13), (12), (15a), (15b), (13c), (13a), (13b))

F^*, F_*	function in equations (A27a) and (A27d)
$\tilde{F}'$	mean slope of F
G	modification factor (eq. (A23))
h	Planck's constant or enthalpy
k	Boltzmann's constant or heat conduction coefficient
L	shock standoff distance
L_c	combined characteristic length
L_{abs}	characteristic absorption length in equation (24b)
L_{dec}	characteristic decay length in equation (24a)
l, m, n	constants (eq. (A4))
P	pressure
q	net radiant heat flux (eq. (5))
q_s	radiative heat flux in upstream direction at shock location (eq. (6a))
q_w	radiative heat flux in downstream direction at wall (eq. (6b))
r	reflectivity
s, t, x'	integration variable
T	absolute temperature
T_e	absolute temperature of air at wall
T_2	absolute temperature behind normal shock wave
$\overline{T}$	ratio of T to T_2
V	velocity behind normal shock
V_∞	flight velocity
x	horizontal coordinate
Γ	parameter (eq. (B2))
ϵ	emissivity or perturbation function (eq. (17))

ϵ', Δ	factors in equation (A25e)
η_1, η_2	constants (eq. (21))
λ	heat-transfer coefficient, $\frac{q}{(1/2)\rho_\infty V_\infty^3}$
ν	frequency
σ	Stefan-Boltzmann constant
ρ	density
μ	absorption coefficient
$\bar{\mu}$	Planck mean absorption coefficient, $\frac{\int_0^\infty \mu_\nu B_\nu \, d\nu}{\int_0^\infty B_\nu \, d\nu}$
τ	optical thickness (eq. (2b))
τ_w	optical thickness for $x = L$

Subscripts

c	conduction
e	gas at the wall
r	radiation
s	shock wave
t	total
w	wall
ν	frequency
2	behind shock
+	upstream direction
-	downstream direction
∞	free stream

Superscripts

'	first derivative with respect to optical thickness
"	second derivative with respect to optical thickness

ANALYSIS

In this section the basic integral equations for the radiative heat fluxes traveling in the upstream and downstream directions are first presented for the case of a nongray gas. These equations are then specialized for the particular case of gray radiation and for the particular boundary conditions of the present problem. By combining these equations with the equations describing the fluid dynamics of the gas flow behind shock waves, the final equations to be solved are obtained. The mathematical techniques employed for their solution are then described.

Equations for One-Dimensional Nongray Radiative Heat Flux

The basic equations for monochromatic radiation of frequency ν between two parallel boundaries are as follows (e.g., refs. 9 and 11):

For the radiative flux in the downstream direction toward the wall

$$q_-(\tau_\nu) = 2\pi \int_0^{\tau_\nu} B_\nu(t) E_2(\tau_\nu - t)\,dt + 2q_-(0) E_3(\tau_\nu) \tag{1}$$

For the radiative flux in the upstream direction toward the shock wave

$$q_+(\tau_\nu) = 2\pi \int_{\tau_\nu}^{\tau_{\nu w}} B_\nu(t) E_2(t - \tau_\nu)\,dt + 2q_+(\tau_{\nu w}) E_3(\tau_{\nu w} - \tau_\nu) \tag{2}$$

where the exponential functions are defined by the integral

$$E_n(t) = \int_0^1 s^{n-2} e^{-t/s}\,ds; \qquad E_1(t) = -E_1(-t) \tag{2a}$$

and the optical path length τ_ν is defined through the equation

$$\tau_\nu = \int_0^x \mu_\nu\,dx' \qquad \text{or} \qquad d\tau_\nu = \mu_\nu\,dx \tag{2b}$$

and the Planck function B_ν is defined through the equation

$$B_\nu(T) = \frac{2h}{c^2} \frac{\nu^3}{e^{h\nu/kT} - 1} \tag{2c}$$

In equations (1) and (2) the integrals represent fluxes from the gas layer itself and the additional terms are fluxes from the boundaries. The radiative flux is integrated over all frequencies as follows:

For the downstream direction

$$q_-(x) = \int_0^\infty q_-(\tau_\nu)\,d\nu \tag{3}$$

For the upstream direction

$$q_+(x) = \int_0^\infty q_+(\tau_\nu)\,d\nu \tag{4}$$

The net radiation flux at any given x position is defined as

$$q(x) = q_+(x) - q_-(x) \tag{5}$$

Basic Equations for Radiative Flux Specialized to Present Problem

Under the assumption made for the present problem of gray radiation, the absorption coefficient μ_ν is independent of frequency ν and so is the optical thickness τ_ν. Also, as is sketched in figure 1, the shock front is assumed to be transparent ($\epsilon_s = r_s = 0$) and the wall is assumed to be an opaque black surface ($\epsilon_w = 1$, $r_w = 0$) with the wall temperature $T_w \ll T_2$. For these conditions equations (1), (2), and (5) reduce to

$$q(\tau) = \int_\tau^{\tau_w} 2\sigma T^4 E_2(t - \tau)\,dt - \int_0^\tau 2\sigma T^4 E_2(\tau - t)\,dt \tag{6}$$

which at the shock wave becomes

$$q_s \equiv q_+(0) = \int_0^{\tau_w} 2\sigma T^4 E_2(t)\,dt \tag{6a}$$

and at the wall becomes

$$q_w \equiv -q_-(\tau_w) = -\int_0^{\tau_w} 2\sigma T^4 E_2(\tau_w - t)\,dt \tag{6b}$$

where the temperature T is a function of the independent variable τ, and τ_w is the optical thickness at the wall.

Since $dE_2(\tau) = -E_1(\tau)d\tau$, differentiation of equation (6) yields

$$dq(\tau) = \left(-4\sigma T^4 + \int_0^{\tau_w} 2\sigma T^4 E_1|t - \tau|\,dt\right) d\tau \tag{7}$$

and the thermal conditions at the shock wave and wall are, respectively,

$$q_s' \equiv q'(0) = -4\sigma T_2^4 + \int_0^{\tau_w} 2\sigma T^4 E_1(t)\,dt \tag{7a}$$

$$q_w' \equiv q'(\tau_w) = -4\sigma T_e^4 + \int_0^{\tau_w} 2\sigma T^4 E_1(\tau_w - t)\,dt \tag{7b}$$

where the prime denotes the derivative with respect to optical thickness.

Combination of Equations for Gas Flow and Radiative Flux

In a one-dimensional steady hypersonic flow such as is being considered, the three basic flow equations are:

continuity

$$d(\rho V) = 0 \tag{8}$$

momentum

$$dP + \rho V\,dV = 0 \tag{9}$$

energy

$$\rho V\,d\left(h + \frac{1}{2}V^2\right) - dq_r - dq_c = 0 \tag{10}$$

or

$$\rho V\left(h + \frac{1}{2} V^2\right) - q_r - k \frac{\partial T}{\partial x} = \text{const.} \tag{10a}$$

For a shock wave moving at hypersonic velocity relative to the undisturbed air, we have the following approximations:

$$\text{(a)} \qquad h_2 \gg \frac{1}{2} V_2{}^2$$

$$\text{(b)} \qquad \frac{-1}{P} \frac{dP}{dx} \sim \frac{1}{V_\infty} \frac{dV}{dx} \ll \frac{1}{L}$$

An important consequence of approximation (b) is that the flow behind the hypersonic normal shock wave is essentially a constant pressure flow. Furthermore, at the very high velocity considered herein, the transport of energy by thermal conduction is disregarded compared to the transport by radiation, so that we have the additional approximation

$$\text{(c)} \qquad q_r \gg k \frac{\partial T}{\partial x}$$

The justification for this assumption will be discussed later in an appendix.

If the above approximations are applied and equation (7) is substituted for dq_r, equation (10) can be written as

$$-\rho_\infty V_\infty \, dh = -dq_r = \left(4\sigma T^4 - \int_0^{\tau_W} 2\sigma T^4 E_1 |t - \tau| dt\right) d\tau \tag{11}$$

The left side of this equation involves the aerothermodynamic variables which may be represented by the dimensionless function F_o' defined as

$$F_o'(P_2, h_2; h) \equiv - \frac{\rho_\infty V_\infty}{2\sigma T_2{}^4} \frac{dh}{d\tau} \tag{11a}$$

Similarly, the right side, which involves the radiation-absorption variables, is represented by the dimensionless function F'

$$F'(\tau_W, \tau) \equiv \frac{1}{2\sigma T_2{}^4} \frac{dq}{d\tau} = 2\bar{T}^4 - \int_0^{\tau_W} \bar{T}^4 E_1 |\tau - t| dt \tag{11b}$$

where $\bar{T}$ is the ratio T/T_2.

At the upstream boundary of the radiation region (adjacent to the shock wave) this last equation becomes

$$F_s' \equiv F'(\tau_w, 0) = 2 - \int_0^{\tau_w} \bar{T}^4 E_1(t)dt \tag{11c}$$

and at the downstream boundary (adjacent to the wall) it becomes

$$F_w' \equiv F'(\tau_w, \tau_w) = 2\bar{T}_e^4 - \int_0^{\tau_w} \bar{T}^4 E_1(\tau_w - t)dt \tag{11d}$$

The integral forms of these equations are

$$F_o(P_2, h_2; h) = \frac{\rho_\infty V_\infty}{2\sigma T_2^4}(h_2 - h) \tag{12}$$

and

$$F(\tau_w, \tau) = \frac{q(0) - q(\tau)}{2\sigma T_2^4}$$

$$= \int_0^{\tau_w} \bar{T}^4 E_2(t)dt + \int_0^{\tau} \bar{T}^4 E_2(\tau - t)dt - \int_\tau^{\tau_w} \bar{T}^4 E_2(t - \tau)dt \tag{13}$$

From equations (6a) and (6b) the upstream value of the flux is

$$F_s = \int_0^{\tau_w} \bar{T}^4 E_2(t)dt \tag{13a}$$

and the downstream value is

$$F_w = \int_0^{\tau_w} \bar{T}^4 E_2(\tau_w - t)dt \tag{13b}$$

The combined or total radiative flux for a given shock standoff distance is

$$F_t = F_s + F_w \tag{13c}$$

In solving the basic equation (11), it is convenient to recast it into a dimensionless form. By dividing both sides of equation (11) by the local temperature T^4, there results

$$\frac{-\rho_\infty V_\infty \, dh}{2\sigma T^4} = \left(2 - \int_0^{\tau_w} \frac{T^4(t)}{T^4} E_1|t - \tau|dt\right) d\tau \tag{14}$$

which, with the definitions,

$$F_1(P_2, h_2; h) \equiv \rho_\infty V_\infty \int_h^{h_2} \frac{dh}{2\sigma T^4} \tag{15a}$$

and

$$F_2(\tau_w, \tau) \equiv \int_0^{\tau} d\tau' \left(2 - \int_0^{\tau_w} \frac{T^4(t)}{T^4} E_1|t - \tau'|dt\right) \tag{15b}$$

becomes

$$F_1(P_2, h_2; h) = F_2(\tau_w, \tau) \tag{15}$$

The derivative of the F_2 function at the shock wave ($\tau = 0$), and at the wall ($\tau = \tau_w$), follow from equation (14).

$$F_{2s}' \equiv F_2'(\tau_w, 0) = 2 - \int_0^{\tau_w} \overline{T}^4(t) E_1(t) dt \tag{16a}$$

$$F_{2w}' \equiv F_2'(\tau_w, \tau_w) = 2 - \frac{1}{\overline{T}_e^4} \int_0^{\tau_w} \overline{T}^4(t) E_1(\tau_w - t) dt \tag{16b}$$

These derivatives represent dimensionless forms of the radiant heat flux passing upstream at the shock, and downstream at the wall, respectively.

OUTLINE OF METHOD OF SOLUTION

Inasmuch as the basic equation (11) is a nonlinear integro-differential equation, a method of solution incorporating successive iterations of approximate solutions is employed. The full development of the analytical method is rather detailed, and is presented in appendix A. In the present section, only the salient or novel features of the method are outlined, and the first approximation, the second approximation, and the conversion from optical to physical coordinates, are briefly described.

First Approximation in Terms of Optical Thickness

A perturbation function $\epsilon(\tau_w, \tau)$ is introduced for the temperature in terms of the following expression:

$$\ln \frac{T^4(t)}{T^4} = \frac{\partial}{\partial t} \ln \frac{T^4(t)}{T^4}\bigg|_{t=\tau} (t - \tau) + \cdots$$

or

$$\frac{T^4(t)}{T^4} = e^{4\frac{T'}{T}(t-\tau) + \cdots} \sim 1 + 4\frac{T'}{T}(t - \tau) + \cdots$$

The function $\epsilon(\tau_w, \tau)$ is then defined as

$$\frac{1}{T^4}\int_0^{\tau_w} \overline{T}^4(t) E_1|t - \tau| dt = [1 + \epsilon(\tau_w, \tau)] \int_0^{\tau_w} E_1|t - \tau| dt \qquad (17)$$

For the case of either small variation of temperature, or of weak absorption,

$$\epsilon(\tau_w, \tau) \sim 0$$

and the integrals appearing in equation (15b) can be evaluated in terms of exponential integral functions

$$F_2(\tau_w, \tau) \simeq \frac{1}{2} - E_3(\tau_w) - E_3(\tau) + E_3(\tau_w - \tau) \qquad (18)$$

The exponential integral $E_3(\tau)$ is further approximated by the exponential function $e^{-2\tau/2}$ which, at $\tau = 0$, has the same value as $E_3(0)$, and the same derivative as $E_3'(0)$; the resulting expression is then multiplied by the normalizing factor $[1 - 2E_3(\tau_w)]/2(1 - e^{-2\tau_w})$ in order for the over-all approximation for F_2 to reduce to the correct value at $\tau = \tau_w$. Thus, as a first approximation, $\epsilon(\tau_w, \tau) = 0$, and the function F_2 is

$$F_2(\tau_w, \tau) \simeq \frac{1 - 2E_3(\tau_w)}{2(1 - e^{-2\tau_w})} [1 - e^{-2\tau_w} - e^{-2\tau} + e^{-2(\tau_w - \tau)}] \qquad (19)$$

This approximation provides a solution for the integrals on the right side of equation (15).

A solution is also required for F_1, the integral term on the left side of equation (15). It is to be noted that the various terms in equations (12) and (15a) are a function only of the thermodynamic

properties as given in figure 2 and are independent of the optical thickness τ. Hence, the integrals of such terms can be readily evaluated from the basic flow charts of various references (e.g., refs. 12, 13, 14, and 15). Functions F_0 and F_1 have been evaluated in this manner and the results are shown as figures 3 and 4. To determine the downstream and upstream radiation fluxes F_W and F_S the temperature as a function of F_1 is expanded in polynomial series as

$$\overline{T}^4 = 1 - \frac{8\sigma T_2^3}{\rho_\infty V_\infty c_{p_2}} F_1 + a_2 F_1^2 + \cdots a_n F_1^n \tag{20}$$

where a_n are constants to be determined. Equations for F_W and F_S can be obtained from equations (13a) and (13b), respectively, after equating F_1 to F_2.

Second Approximation for the Solution in Terms of the Optical Thickness

For the second approximation, a modified form of the F_2 function is employed

$$F_2(\tau_W, \tau) = d[1 - e^{-\eta_2 \tau_W} - e^{-\eta_1 \tau} + e^{-\eta_2(\tau_W - \tau)}] \tag{21}$$

from which the slopes at both ends are obtained as

$$F_{2S}' \simeq d(\eta_1 + \eta_2 e^{-\eta_2 \tau_W}) \tag{21a}$$

$$F_{2W}' \simeq d(\eta_1 e^{-\eta_1 \tau_W} + \eta_2) \tag{21b}$$

The values of the constants d, η_1, and η_2 are determined from an iteration of the first approximation. It has been found expedient, because of the singularity in $F''(\tau_W, \tau)$ at $\tau = \tau_W$, to introduce a mean slope $\tilde{F}_W'$ instead of F_{2W}' in order to compensate for small but sudden changes of temperature near the wall.

Conversion From Optical Thickness to Physical Dimensions

With the solution established in terms of optical thickness it is a relatively simple matter to convert to the corresponding physical coordinates. For strictly gray radiation the absorption coefficient μ is constant, but for air radiation μ varies; and hence some mean value

should be used. The Planck mean $\bar{\mu}$ is employed herein. From the definition of optical thickness for gray gas (eq. (2b)), we have

$$d\tau = \bar{\mu}\, dx$$

from which it follows that

$$x = \int_0^{\tau} \frac{d\tau}{\bar{\mu}} \tag{22}$$

In applying this equation to a flow with a shock detachment distance L, the basic assumption (6) of the present paper is employed

$$L = x_w \tag{23}$$

Thermodynamic properties behind a normal shock are presented in figures 5 and 6, and corresponding values for the absorption coefficient $\bar{\mu}$ are computed from data in references 16 and 17 and presented in figure 7. The variation of temperature over the distance x behind the shock wave is obtained from equation (19) or (21) and the data of figure 3.

RESULTS AND DISCUSSION

Prior to the presentation of results from solutions of the integro-differential equation for the radiative heat flux, several auxiliary charts will be presented. Useful aerothermodynamic charts for applying the present results to a given problem of atmosphere entry are presented in figures 5 and 6; these give the values of temperature, pressure, and density behind normal shock waves for various flight conditions. The basic data for the equilibrium radiation intensity per unit volume are given in figure 8; these data were obtained by combining the results of references 16 and 17. For purposes of comparison, a summary plot of the radiative heat transfer to a stagnation point of a hemisphere, as obtained from the work of reference 3 for the case of no absorption, is presented in figure 9. (It is noted that a correction factor of 1 to 0.8 for the spherical segment of the gas cap as opposed to an infinite slab has been included in the data of these figures.)

In order to delineate the flight conditions under which absorption is important it is convenient to introduce the idea of a characteristic length L_c. The relative magnitudes of L_c and of the shock standoff distance L provide a convenient means of marking the boundaries of the domains wherein the decay and the absorption of radiation are significant. A characteristic decay length, L_{dec}, is introduced as

$$L_{dec} = \frac{\rho_\infty V_\infty h_2}{4\bar{\mu}\sigma T_2^4} \simeq \frac{\frac{1}{2}\rho_\infty V_\infty^3}{E_{t_2}} \tag{24a}$$

where L_{dec} is the length required to lose all energy by radiation of constant intensity behind a normal shock wave. A characteristic absorption length, L_{abs}, is defined as

$$L_{abs} = \frac{1}{2\bar{\mu}} \tag{24b}$$

and is the length required to reach the black body radiation limit. At relatively high densities, $L_{abs} \ll L_{dec}$, so that absorption dominates decay and $L_c \simeq L_{abs}$; but at relatively low densities, $L_{dec} \ll L_{abs}$ so that decay dominates absorption and $L_c \simeq L_{dec}$. By fairing between these two characteristic lengths in intermediate regions, a single characteristic length L_c has been obtained for the entire flight domain. Curves of combined characteristic lengths are presented in figure 10. If the shock detachment distance L is such that

$$L \leq \frac{1}{10} L_c \tag{25}$$

then the nondecay-nonabsorption regime would be applicable and the radiation heat flux would be that of an isothermal gas. At the opposite extreme of very high pressures, namely, $P_2 > 10^2$ atm, where the absorption is strong and the characteristic length L_c is such that

$$L_c \leq \frac{1}{10} L \tag{26}$$

the radiation heat flux would be essentially that of black body radiation at the local temperature (which would vary between the shock and the wall).

Before determining the degree of refinement required to estimate accurately the radiative flux by the first approximation, the accuracy of the second approximation is investigated. Temperature distributions as determined by the second approximation and by equations (12) and (13) are shown in figure 11. When the second approximation (continuous curved line) is used as input into these equations, the square points are obtained as the output. The physical condition presented in figure 11 is a typical case where radiation absorption, as well as the interdependence of the radiation term and the enthalpy term of the energy equation, is important. As may be seen from the close agreement of curves and points in figure 11, the results of the second approximation are very accurate. Hence, the second approximation, which is an iterated solution based upon the first approximation, may be considered as nearly exact.

The first approximation is less accurate than the second, but is adequate for most conditions. Curves for the radiation heat flux according to the first and second approximations are shown in figure 12.

The difference between the two approximations is less than 4 percent. It should be noted that at either higher or lower pressures the radiation fluxes, as calculated from the two approximations, will approach each other even more closely, inasmuch as these conditions correspond to either smaller temperature variations or to weaker absorption effects behind the shock. The first approximation, which is rather simple to evaluate, is therefore considered to be sufficiently accurate to estimate the radiative heat transfer.

The principal results of this report are presented in figures 13 and 14. The radiative flux F_S at the shock wave and F_W at the wall as determined from equations (13a) and (13b) according to the first approximation are plotted as functions of τ_W in figure 13. Figure 14 shows a typical comparison of the radiation flux for the case wherein absorption and decay are neglected with the case wherein both absorption and decay are considered. The solid straight line represents the flux with no absorption or decay, corresponding to a constant temperature behind the shock. As τ_W increases, F_S and F_W curve away from this line as a result of the decay phenomenon; these curves become a plateau as τ_W is increased further as a result of the absorption phenomenon. It is noted that the flux at the wall, F_W, for an optically thick layer is larger than the local black body radiation at the wall. This is due to the fact that the temperature gradient at the wall is negative, and the gas temperature everywhere in the shock layer exceeds T_e. It is also noted that the departure of the F_S curve from the F_W curve is a manifestation of decay and absorption effects, inasmuch as F_W would equal F_S if there were negligible decay or no absorption. Since both of these curves bend away from the straight line (representing no decay or absorption) by a great amount, as well as deviate from each other by a substantial amount, it follows that the effects of both decay of radiation and absorption of radiation are important in this case.

The results in terms of the coefficient of heat transfer λ and shock detachment distance L are presented in figure 15. The definition of the dimensionless heat-transfer coefficient is

$$\lambda = \frac{q}{\frac{1}{2}\rho_\infty V_\infty^3}$$

A crossplot of the various calculations for the heat-transfer coefficient at a given shock detachment distance is also presented in figure 16. It is noted that in the lower right portion of each part of figure 16 where $T_2 > 15{,}000^\circ$ K (see fig. 6) the curves shown here have been extrapolated by using the black body radiation limit as a guide.

From figure 16 several conclusions of practical interest may be drawn. If attention is confined to the altitude range of severe heating for shallow entry trajectories of manned vehicles (60 to 80 km), it is

seen that, for entry velocities of about 11 km/sec (corresponding to entry upon return from the moon), neither decay nor absorption of radiation would be important for L of 1 foot or less. At higher entry velocities of about 15 km/sec (corresponding to entry upon return from a short-time trajectory from Mars), decay of radiation would be important but absorption would not. For objects such as large meteorites, however, which enter at higher entry velocities and also at relatively steep angles, the most severe heating occurs at altitudes of about 20 to 40 km, where both decay and absorption are major factors in determining the radiative heat flux to the body.

In regard to the limitations of the present calculations and to their possible extensions the following observations are made:

(1) The calculations become questionable at very high velocities where the gas cap temperature is so high that intense ultraviolet radiation emitted upstream through the shock wave is absorbed by the oncoming air. Under such conditions the absorption and re-emission upstream of the shock wave would modify the results.

(2) The assumption of local aerothermal equilibrium behind the shock wave is valid at the relatively high pressures and temperatures where absorption is important, but it would not be valid at lower densities where nonequilibrium phenomena have been demonstrated to be important (see ref. 18).

(3) At temperatures other than those considered herein the transport of heat by thermal conduction may be important. The results discussed in appendix B show, however, that for the range of variables considered herein, thermal conduction is small compared to radiation heat transfer.

(4) The accuracy of the gray gas approximation for air has not yet been evaluated.

CONCLUDING REMARKS

Within the framework of the assumptions made, it is found that rather simple calculations of both the radiative heat flux downstream to the wall, and of the radiative heat flux upstream from the gas behind a normal shock wave, provide a satisfactory solution to the problem of a nonisothermal, absorbing, emitting gas. It is noted that at very high velocities and large shock detachment distances, the calculated radiative heat flux, compared to that of the isothermal approximation, is much lower when decay and/or absorption are considered. In general, the characteristic length provides a good guide to the appropriate radiative regime (isothermal, decay, or absorption) in which a given entry vehicle

operates. For manned vehicles entering along shallow trajectories at twice the satellite velocity, for example, the effect of decay can be significant, and for a large meteorite, or instrument-return vehicle, entering along a steep trajectory, the effect of absorption can also be significant.

Ames Research Center
National Aeronautics and Space Administration
Moffett Field, Calif., May 21, 1962

APPENDIX A

METHOD OF SOLUTION

EVALUATION OF $\bar{T}$ IN TERMS OF THE FUNCTION F_1

One of the equations to be solved for the radiative flux is

$$F_1(P_2,\ h_2;\ h) = F_2(\tau_w,\ \tau) \tag{15}$$

From aerothermodynamic charts, such as presented in references 12, 14, or 15, equation (15a), the left hand side of equation (15), can be evaluated for a constant pressure process.

$$F_1(P_2,\ h_2;\ h) \equiv \rho_\infty V_\infty \int_h^{h_2} \frac{dh}{2\sigma T^4} = \rho_\infty V_\infty \int_T^{T_2} \frac{c_p\ dT}{2\sigma T^4} \tag{15a}$$

The enthalpy at constant pressure as deduced from reference 15 is plotted in figure 2 as a function of temperature. The variations in temperature with F_1 are shown in figure 3. These were obtained from the enthalpy curves in figure 2 by approximating them by a third degree polynomial of temperature over intervals of 1000° K.

From figure 3 $T^4/T_2{}^4 = \bar{T}^4$ can be readily expressed in terms of F_1.

$$\bar{T}^4 = \sum_{n=0}^{N} a_n F_1{}^n \tag{A1}$$

For the present work, N = 3 represents a sufficiently accurate approximation

$$\bar{T}^4 = a_0 + a_1 F_1 + a_2 F_1{}^2 + a_3 F_1{}^3 \tag{A2}$$

where a_n will be denoted as

$$a_0 = 1$$

$$a_1 = a = \left.\frac{d\bar{T}^4}{dF_1}\right|_{F_1=0} = -\frac{8\sigma T_2{}^3}{\rho_\infty V_\infty c_{p_2}}$$

$$a_2 = b$$

$$a_3 = c$$

Let $F_1 = F_2$ as given in equation (15), and F_2 from equation (21) as $F_2 = d[1 - e^{-\eta_2\tau_w} - e^{-\eta_1\tau} + e^{-\eta_2(\tau_w-\tau)}]$, then (A2) becomes

$$\overline{T}^4 = A - B_o e^{-\eta_2\tau_w} e^{-l\tau} + B_1 e^{-\eta_2\tau_w} e^{-m\tau} - B_1 e^{-2\eta_2\tau_w} e^{-n\tau} - Be^{-\eta_1\tau} + Be^{-\eta_2(\tau_w-\tau)}$$
$$+ Ce^{-2\eta_1\tau} + Ce^{-2\eta_2(\tau_w-\tau)} - De^{-3\eta_1\tau} + De^{-3\eta_2(\tau_w-\tau)} \qquad (A3)$$

where

$$\left.\begin{aligned} l &= \eta_1 - \eta_2 \\ m &= 2\eta_1 - \eta_2 \\ n &= \eta_1 - 2\eta_2 \end{aligned}\right\} \qquad (A4)$$

$$\left.\begin{aligned} A &= 1 + adf + bd^2f^2 + cd^3f^3 \\ B_o &= 2bd^2 + 6cd^3f \\ B_1 &= 3cd^3 \\ B &= ad + 2bd^2f + 3cd^3f^2 \\ C &= bd^2 + 3cd^3f \\ D &= cd^3 \\ f &= 1 - e^{-\eta_2\tau_w} \end{aligned}\right\} \qquad (A5)$$

For $\eta_1 = \eta_2 = 2$ the following relations are used in equation (A3)

$$A - B_o \text{ as } A \quad \text{and} \quad B - B_1 \text{ as } B \qquad (A6)$$

Equations (A3) to (A6) provide the evaluation of function $\overline{T}^4$.

In evaluating the radiative fluxes from equations (13a), (13b), and (13c), and the derivatives of the flux from equations (11c) and (11d) with equation (A3), many terms involving the integral of a product of an exponential and an exponential integral function are encountered. Such integrals have been evaluated from references 19 and 20.

EVALUATION OF INTEGRALS INVOLVING $E_2(\tau)$ AND $E_1(\tau)$

$$\int_0^{\tau_w} e^{-\eta\tau} E_2(\tau)\,d\tau = \int_0^{\tau_w} e^{-\eta(\tau_w-\tau)} E_2(\tau_w - \tau)\,d\tau$$

$$= \frac{1}{\eta^2}\left\{\frac{1}{e^{\eta\tau_w}}\left[E_1(\tau_w) - \eta E_2(\tau_w)\right]\right.$$

$$\left. + \ln(\eta + 1) - \eta - E_1(\eta + 1)\tau_w\right\} \qquad \text{(A7a)}$$

$$\int_0^{\tau_w} e^{-\eta(\tau_w-\tau)} E_2(\tau)\,d\tau = \int_0^{\tau_w} e^{-\eta\tau} E_2(\tau_w - \tau)\,d\tau$$

$$= \frac{1}{\eta^2}\left\{E_1(\tau_w) + \eta E_2(\tau) + \frac{1}{e^{\eta\tau_w}}\right.$$

$$\left.[-\ln(\eta - 1) - \eta + E_i(\eta - 1)\tau_w]\right\} \qquad \text{(A7b)}$$

$$\int_0^{\tau_w} E_2(\tau)\,d\tau = \int_0^{\tau_w} E_2(\tau_w - \tau)\,d\tau = \frac{1}{2} - E_3(\tau_w) \qquad \text{(A7c)}$$

$$\int_0^{\tau_w} e^{-\eta\tau} E_1(\tau)\,d\tau = \int_0^{\tau_w} e^{-\eta(\tau_w-\tau)} E_1(\tau_w - \tau)\,d\tau$$

$$= \frac{1}{\eta}\left[\ln(1 + \eta) + E_1(1 + \eta)\tau_w - e^{-\eta\tau_w} E_1(\tau_w)\right] \qquad \text{(A8a)}$$

$$\int_0^{\tau_w} e^{-\eta(\tau_w-\tau)} E_1(\tau)\,d\tau = \int_0^{\tau_w} e^{-\eta\tau} E_1(\tau_w - \tau)\,d\tau$$

$$= \frac{1}{\eta}\left[-e^{-\eta\tau_w}\ln(\eta - 1) + e^{-\eta\tau_w} E_i(\eta - 1)\tau_w + E_1(\tau_w)\right] \qquad \text{(A8b)}$$

$$\int_0^{\tau_w} E_1(\tau)d\tau = \int_0^{\tau_w} E_1(\tau_w - \tau)d\tau = 1 - E_2(\tau_w) \qquad \text{(A8c)}$$

The following relations are used:

if $\eta < 1$

$$-\ln(\eta - 1) + E_i(\eta - 1)\tau_w = -\ln(1 - \eta) - E_1(1 - \eta)\tau_w$$

if $\eta = 1$

$$-\ln(\eta - 1) + E_i(\eta - 1)\tau_w = \gamma + \ln \tau_w$$

where γ = Eulers constant (=0.57722).

For simplicity of calculations numerical values associated with equations (A7a) to (A8c) have been prepared for η from 0.1 to 9.0 with 0.1 intervals.

FORMULATION OF F AND F' FUNCTION

Equations (13a), (b), and (c) upon the introduction of equation (A3) and the integrals evaluated in the previous section become the following:

By employing the following symbolic notation for the integral evaluated in equations (A7a) to (A7c)

(A7a) $\equiv$ (I)	e.g.,	$\eta = 1$ in (A7a) $\equiv (I)_1$
(A7b) $\equiv$ (II)		$\eta = \eta_2$ in (A7a) $\equiv (I)_2^1$
(A7c) $\equiv$ (III)		$\eta = 2\eta_1$ in (A7b) $\equiv (II)_1^2$
		$\eta = 3\eta_2$ in (A7a) $\equiv (I)_2^3$ etc.

then

$$F_S = A(III) - B_o(I)_1 + B_1[(I)_m - (I)_n] - B[(I)_2^1 - (II)_2^1] + C[(I)_1^2 + (II)_2^2] - D[(I)_1^3 - (II)_2^3] \qquad \text{(A9)}$$

$$F_W = A(III) - B_o(II)_1 - B_1[(II)_n - (II)_m] + B[(I)_2^1 - (II)_1^1] + C[(I)_2^2 + (II)_1^2] + D[(I)_2^3 - (II)_1^3] \qquad \text{(A10)}$$

$$F_t = F_s + F_w$$

$$= 2A(III) - B_o[(I)_l + (II)_l] + B_1\{(I)_m + (II)_m - [(I)_n + (II)_n]\}$$
$$+ C[(I)_1^2 + (II)_1^2 + (I)_2^2 + (II)_2^2] - B\{(I)_1^1 + (II)_1^1 - [(I)_2^1 + (II)_2^1]\}$$
$$- D\{(I)_1^3 + (II)_1^3 - [(I)_2^3 + (II)_2^3]\} \qquad (A11)$$

Also, equations (11c) and (d) with the symbolic notation

$$(A8a) \equiv [I]$$

$$(A8b) \equiv [II]$$

$$(A8c) \equiv [III]$$

become

$$F_s' = 2 - \Big(A[III] - B_o[I]_l + B_1\{[I]_m - [I]_n\} - B\{[I]_1^1 - [II]_2^1\}$$
$$+ C\{[I]_1^2 + [II]_2^2\} - D\{[I]_1^3 - [II]_2^3\}\Big) \qquad (A12)$$

$$F_w' = 2\bar{T}_e^4 - \Big(A[III] - B_o[II]_l - B_1\{[II]_n - [II]_m\} + B\{[I]_2^1 - [II]_1^1\}$$
$$+ C\{[I]_2^2 + [II]_1^2\} + D\{[I]_2^3 - [II]_1^3\}\Big) \qquad (A13)$$

For the first approximation ($\eta_1 = \eta_2 = 2$) F_s, F_w, and F_t with condition (A6) become

$$F_s = A(III) - B[(I)_1^1 - (II)_1^1] + C[(I)_1^2 + (II)_1^2] - D[(I)_1^3 - (II)_1^3] \qquad (A14)$$

$$F_w = A(III) + B[(I)_1^1 - (II)_1^1] + C[(I)_1^2 + (II)_1^2] + D[(I)_1^3 - (II)_1^3] \qquad (A15)$$

$$F_t = 2A(III) + 2C[(I)_1^2 + (II)_1^2] \qquad (A16)$$

Also, F_s' and F_w' can be written

$$F_s' = 2 - \Big(A[III] - B\{[I]_1^1 - [II]_1^1\} + C\{[I]_1^2 + [II]_1^2\}$$
$$- D[I]_1^3 - [II]_1^3\}\Big) \qquad (A17)$$

$$F_w' = 2\bar{T}_e^4 - \Big(A[III] + B\{[I]_1^1 - [II]_1^1\} + C\{[I]_1^2 + [II]_1^2\} + D\{[I]_1^3 - [II]_1^3\}\Big) \tag{A18}$$

By definition

$$F_{2s}' = F_s' \tag{A19}$$

$$F_{2w}' = \frac{1}{\bar{T}_e^4} F_w' \tag{A20}$$

F_2 Function for First Approximation

As a first approximation, $\epsilon(\tau, t) \sim 0$ and F_2 are readily evaluated in terms of exponential integral functions

$$F_2(\tau_w, \tau) \simeq \frac{1}{2} - E_3(\tau_w) - E_3(\tau) + E_3(\tau_w - \tau) \tag{18}$$

However, due to difficulties associated with evaluation of expressions, such as $\int_0^{\tau_w} E_3^n(\tau_w - \tau)E_2(\tau)d\tau$, the function $E_3(\tau)$ is further approximated by the simple exponential function $e^{-2\tau}/2$ which, at $\tau = 0$, has the same value as $E_3(0)$, and the same derivative as $E_3'(0)$; to compensate for this approximation, a normalizing factor $1 - 2E_3(\tau_w)/2(1 - e^{-2\tau_w})$ is applied in order that $F_2(\tau_w, \tau_w)$ reduce to the proper value of $1 - 2E_3(\tau_w)$. The result for the first approximation is

$$F_2(\tau_w, \tau) \simeq \frac{1 - 2E_3(\tau_w)}{2(1 - e^{-2\tau_w})}\left[1 - e^{-2\tau_w} - e^{-2\tau} + e^{-2(\tau_w - \tau)}\right] \tag{19}$$

Modification Factor $G(\tau_w)$ in Second Approximation

The method of determining the mean value of $\tilde{F}_w'$, mentioned earlier in the outline of solution, is described in this section. The second derivative of $F(\tau_w, \tau)$ can be derived from equation (11b) as

$$F''(\tau_w, \tau) = 8\bar{T}^3 \frac{\partial \bar{T}}{\partial \tau} + \int_0^{\tau} \bar{T}^4 E_0(\tau - t)dt - \int_{\tau}^{\tau_w} \bar{T}^4 E_0(t - \tau)dt \tag{A21}$$

Then

$$F_s'' = 8 \left.\frac{\partial \bar{T}}{\partial \tau}\right|_{\tau=0} - \int_0^{\tau_w} \bar{T}^4 E_0(t)\,dt \tag{A22a}$$

$$F_w'' = 8\bar{T}_e^{\,3} \left.\frac{\partial \bar{T}}{\partial \tau}\right|_{\tau=\tau_w} + \int_0^{\tau_w} \bar{T}^4 E_0(\tau_w - t)\,dt \tag{A22b}$$

From the above equations it is apparent that F'' at both boundaries is infinite, and these singularities (especially at $\tau = \tau_w$) create an infinite gradient of temperature, even though the change in T is very small; equation (21b) remains finite at both ends. To compensate for this effect, a modification factor G is introduced to adjust F_w' by the relationship

$$\tilde{F}_w' = G(\tau_w) F_w' \tag{A23}$$

The value of F' at $\tau = 0.95\tau_w$ is found to be a good average value to use instead of the actual value at the end. It can be obtained approximately as follows:

From equation (11b)

$$F'(\tau_w, \tau) = 2\bar{T}^4 - \int_0^{\tau_w} \bar{T}^4 E_1|\tau - t|\,dt \sim \bar{T}^4\left(2 - \int_0^{\tau_w} E_1|\tau - t|\,dt\right)$$

or

$$F'(\tau_w, \tau) \sim \bar{T}^4[E_2(\tau) + E_2(\tau_w - \tau)]$$

then

$$G(\tau_w) \equiv \frac{F'(\tau_w, 0.95\tau_w)}{F_w'} \approx \frac{\bar{T}^4(0.95\tau_w)[E_2(0.95\tau_w) + E_2(0.05\tau_w)]}{\bar{T}_e^{\,4}[E_2(\tau_w) + 1]} \tag{A24}$$

where $T(0.95\tau_w)$ and T_e are found from the first approximation, and $G(\tau_w)$ is limited by the inequality

$$G(\tau_w) \geq 1/2$$

To maintain some slope at the end, for example τ_w at ∞, the mean value of $G(\infty) = 1/2$ is used instead of $G(\infty) = 0$. It was noted that the slope around $\tau = 0$ was smooth enough that no significant correction was required.

PROCEDURE FOR DETERMINING SECOND APPROXIMATION

The second approximation is obtained as follows:

Equations (A16), (A12), and (A13), with the use of the first approximation (eq. (19)), yield the following quantities:

$$\left.\begin{aligned} &F_t \rightarrow F_{2w} = F_2(\tau_w, \tau_w) \text{ from figure 4} \\ &F_s' \rightarrow F_{2s}' \\ &F_w' \rightarrow F_{2w}' \rightarrow \tilde{F}_{2w}' \quad \text{equations (A23) and (A24)} \end{aligned}\right\} \qquad \text{(A25a)}$$

Equations (21), (21a), and (21b) are then matched with the above conditions in (A25a) to determine the constants d, η_1, and η_2. The following outline illustrates the calculation procedure:

(a) Assume $d = \dfrac{1 - 2E_3(\tau_w)}{2(1 - e^{-\eta_1 \tau_w})}$ as given at equation (19), and $\eta_1 = 2$

(b) Calculate η_2 from equation (21b) as

$$\eta_2 = \frac{\tilde{F}_{2w}'}{d} - \eta_1 e^{-\eta_1 \tau_w}, \text{ and find } e^{-\eta_2 \tau_w} \text{ and } \eta_2 e^{-\eta_2 \tau_w} \qquad \text{(A25b)}$$

(c) Calculate η_1 from equation (21a) as

$$\eta_1 = \frac{F_{2s}'}{d} - \eta_2 e^{-\eta_2 \tau_w}, \text{ and also } e^{-\eta_1 \tau_w} \text{ and } \eta_1 e^{-\eta_1 \tau_w} \qquad \text{(A25c)}$$

(d) Repeat (b) and (c) until η_1 and η_2 converge to two significant figures

(e) Then compute a new d from

$$d = \frac{F_{2w}}{(2 - e^{-\eta_1 \tau_w} - e^{-\eta_2 \tau_w})} \qquad \text{(A25d)}$$

and repeat procedures (b) and (c) until d, η_1, and η_2 converge.

A set of constants in (A5) are then computed from d, η_1, and η_2 obtained above, and new values of F_t, F_s', and F_w' are obtained from (A11), A12), and (A13).

The entire above procedure is repeated until d, η_1, and η_2 coincide with the previous iteration. It was found that F_S' and F_W' obtained from the first approximation always gave sufficient convergence so that no further iteration upon these values was necessary. Also, it was found that the precise accuracy of these quantities was not so significant compared with that of F_t.

When η_1 and η_2 are stable or given, d can be estimated from (A5) in the following way: Let

$$\epsilon' = \frac{\Delta d}{d} \ll 1$$

Then differentiation of (A5) with respect to d,

$$\left.\begin{aligned} \Delta A &\sim (adf + 2bd^2f^2 + 3cd^3f^3)\epsilon' \\ \Delta B_0 &\sim (4bd^2 + 18cd^3f)\epsilon' \\ \Delta B_1 &\sim (9cd^3)\epsilon' \\ \Delta B &\sim (ad + 4bd^2f + 9cd^3f^2)\epsilon' \\ \Delta C &\sim (2bd^2 + 9cd^3f)\epsilon' \\ \Delta D &\sim (3cd^3)\epsilon' \end{aligned}\right\} \qquad \text{(A25e)}$$

These values are substituted into equation (A11) for an arbitrary value of d near the original value, and corresponding values of F_t are plotted against F_2 $(=F_1)$ in figure 4. Intersection of the plotted curve with the original curve is the point where d is determined from F_2.

EVALUATION OF RADIATIVE FLUXES FOR SPECIAL CASES

For the case of either a small or a large optical thickness, the calculation of the radiative flux by the first approximation becomes rather simple.

$$\tau_W \ll 1$$

By use of approximation

$$E_3(\tau) \sim \frac{1}{2} - \tau \qquad \text{(A26a)}$$

equation (18) becomes

$$F_2(\tau_W, \tau) = \frac{1}{2} - E_3(\tau_W) = E_3(\tau) + E_3(\tau_W - \tau) \simeq 2\tau \qquad \text{(A26b)}$$

and it follows after $F_1 = F_2$

$$\overline{T}^4 = 1 + a_1F_1 + a_2F_1^2 + a_3F_1^3 + \cdots \simeq 1 + 2a_1\tau + \cdots \qquad \text{(A26c)}$$

then fluxes at both ends are

$$F_S = F_W = \int_0^{\tau_W} \overline{T}^4 E_2(\tau)\,d\tau = \int_0^{\tau_W} \overline{T}^4 E_2(\tau_W - \tau)\,d\tau$$

$$\simeq \int_0^{\tau_W} (1 + 2a_1\tau) E_2(\tau)\,d\tau = \frac{1}{2} - E_3(\tau_W) - 2a_1\left[-\tau_W E_3(\tau_W) - E_4(\tau_W) + \frac{1}{3}\right]$$

$$\simeq \tau_W \qquad \text{(A26d)}$$

This result clearly is the appropriate one for the case of either the isothermal or the decay approximation.

$$\tau_W \gg 1$$

In evaluation of the flux at the shock F_S, terms $-E_3(\tau_W) + E_3(\tau_W - \tau)$ can be dropped from the function F_2 since crossproducts of these terms with exponential integral $E_2(\tau)$ become negligible for $\tau_W \gg 1$. Thus, it follows after definition of F^*

$$F^*(\tau) = \frac{1}{2} - E_3(\tau) \qquad \text{(A27a)}$$

that

$$F_S = \int_0^{F^*(\tau_W)} (1 + a_1F^* + a_2F^{*2} + a_3F^{*3} + \cdots)\,dF^*$$

$$= F(\tau_W) + \frac{a_1}{2} F^{*2}(\tau_W) + \frac{a_2}{3} F^{*3}(\tau_W) + \frac{a_3}{4} F^{*4}(\tau_W) + \cdots \qquad \text{(A27b)}$$

As $E_3(\tau_W) \to 0$

$$F_S \simeq \frac{1}{2} + \frac{1}{8} a_1 + \frac{1}{24} a_2 + \frac{1}{64} a_3 + \cdots \qquad \text{(A27c)}$$

Similarly the term $-E_3(\tau_w) + E_3(\tau)$ can be dropped from F_2 for the flux at the wall F_w, and after definition of F_* it follows

$$F_*(\tau) = \frac{1}{2} + E_3(\tau_w - \tau) \tag{A27d}$$

$$F_w = \int_{F_*(0)}^{1} (1 + a_1 F_* + a_2 F_*^2 + a_3 F_*^3 + \ldots) dF_*$$

$$= 1 - F_*(0) + \frac{a_1}{2}[1 - F_*^2(0)] + \frac{a_2}{3}[1 - F_*^3(0)] + \frac{a_3}{4}[1 - F_*^4(0)] + \ldots \tag{A27e}$$

Asymptotically

$$F_w = \frac{1}{2} + \frac{3}{8} a_1 + \frac{7}{24} a_2 + \frac{15}{64} a_3 + \ldots \tag{A27f}$$

Then the total radiative flux F_t becomes

$$F_t = F_s + F_w$$

$$= 1 + \frac{1}{2} a_1 + \frac{1}{3} a_2 + \frac{1}{4} a_3 + \ldots \tag{A27g}$$

Fluxes calculated by both equations (A27b) and (A27e) provide a good and quick estimate of an optically thick case for $\bar{T}^4 > 1/2$. Furthermore, it is noted that the expansion of equations (A27b) and (A27e) in terms of equation (A26a) produced an identical result as equation (A26d), which is for the optically thin case. Thus, it is suggested that the above equations may well be applicable for all τ_w within the limitation of $\bar{T}^4 > 1/2$.

APPENDIX B

MAGNITUDE OF CONDUCTION HEAT RELATIVE TO RADIANT HEAT

The magnitude of the conduction heat transfer in equation (10a) can be estimated from equation (11c), with the thermal conductivity of air obtained from reference 21, as follows:

$$\frac{\partial T}{\partial x} = \frac{dT}{dF_2}\frac{dF_2}{dF}\frac{\partial F}{\partial \tau}\frac{d\tau}{dx}$$

but

$$\left.\frac{dT}{dF_2}\right|_{F_2=0} = \frac{-2\sigma T_2{}^3}{\rho_\infty V_\infty c_{p_2}}; \quad \left.\frac{dF_2}{dF}\right|_{F=0} = 1; \quad \left.\frac{\partial F}{\partial \tau}\right|_{\tau=0} = F_s'; \quad \frac{d\tau}{dx} = \bar{\mu}_2$$

hence

$$-\left(k\frac{\partial T}{\partial x}\right)_{max} = -k\left.\frac{\partial T}{\partial x}\right|_{x=0} = \left(\frac{k_2\bar{\mu}_2}{c_{p_2}}\right)\left(\frac{2\sigma T_2{}^4}{\rho_\infty V_\infty}\right)F_s' \tag{B1}$$

Let

$$\Gamma \equiv \frac{k\frac{\partial T}{\partial x}}{2\sigma T_2{}^4 F_t} \tag{B2}$$

Then from equation (B1)

$$\Gamma = \frac{k_2\bar{\mu}_2}{\rho_\infty V_\infty c_{p_2}}\frac{F_s'}{F_t} \tag{B3}$$

For $\tau_w \gg 1$

$$F_s' \sim 1$$

$$F_t \sim 1$$

It is found from reference 21 that

$$\Gamma \sim \frac{k_2\bar{\mu}_2}{\rho_\infty V_\infty c_{p_2}} \ll 1 \quad \text{for} \quad T_2 \leq 15{,}000^\circ \text{ K} \tag{B4}$$

For $\tau_w \ll 1$

$$F_s' \sim 2$$

$$F_t \sim 2\tau_w$$

or

$$\Gamma \sim \frac{k_2}{\rho_\infty V_\infty c_{p_2} L} \tag{B5}$$

The above parameter can be large for sufficiently small values of shock detachment distance L where thermal conduction begins to be important. This boundary could be considered along with the boundaries already shown in figure 10. However, L, in most practical cases, will not be less than 10^{-2} cm. For such conditions the contribution of heat conduction to the energy equation is negligible since $\Gamma \ll 1$. (It is noted that these calculations do not consider the boundary layer where viscous effects are large.)

For example:

$T_2 < 15{,}000^\circ$ K $P_2 = 1{,}000$ atm $\Gamma \ll 1$ for $L \gg 10^{-5}$ cm

$= 100$ 10^{-4}

$= 10$ 10^{-3}

$= 1$ 10^{-2}

REFERENCES

1. Kivel, B.: Radiation From Hot Air and Stagnation Heating. Research Rep. 79, AVCO Res. Lab., Oct. 1959.

2. Goulard, R.: The Coupling of Radiation and Convection in Detached Shock Layers. Bendix Product Div., Applied Sciences Lab., April 1959.

3. Yoshikawa, Kenneth K., and Wick, Bradford H.: Radiative Heat Transfer During Atmosphere Entry at Parabolic Velocity. NASA TN D-1074, 1961.

4. Allen, H. Julian: Problems in Atmospheric Entry From Parabolic Orbits. Jour. of Japan Soc. for Aero. and Space Sci., vol. 9, no. 85, Feb. 1961, pp. 43-50.

5. Allen, H. Julian: On the Motion and Ablation of Meteoric Bodies. Aero. and Astro; Proc. Durand Centennial Conf., ed. by N. J. Hoff and W. G. Vincenti, Pergamon Press, N. Y., 1960, pp. 378-416.

6. Chapman, Dean R.: An Approximate Analytical Method for Studying Entry Into Planetary Atmospheres. NASA TR R-11, 1959.

7. Viskanta, R.: Heat Transfer in Thermal Radiation Absorbing and Scattering Media. ANL-6170, Argonne National Lab., May 1960.

8. Pomerantz, Jacob: The Influence of the Absorption of Radiation in Shock Tube Phenomena. NAVORD Rep. 6136, Aug 15, 1958.

9. Goulard, R., and Goulard, M.: One Dimensional Energy Transfer in Radiant Media. Int'l Jour. Heat Mass Transfer, vol. 1, 1960, pp. 81-91.

10. Chandrasekhar, S.: Radiative Transfer. Clarendon Press, Oxford, 1950.

11. Kourganoff, V.: Basic Methods in Transfer Problems. Clarendon Press, Oxford, 1952.

12. Hochstim, A. R.: Gas Properties Behind Shocks at Hypersonic Velocities. Pt. I - Normal Shocks in Air. Convair ZPh(GP) 002, Jan. 30, 1957.

    Hochstim, A. R.: Gas Properties Behind Shocks at Hypersonic Velocities. Pt. II - Introduction to General Thermodynamics of a Real Gas. Convair ZPh 003, May 15, 1957.

    Hochstim, A. R., and Arave, Russell J.: Gas Properties Behind Shocks at Hypersonic Velocities. Pt. III - Various Thermodynamical Properties of Air. Convair ZPh 004, June 14, 1957.

13. Ziemer, R. W.: Extended Hypervelocity Gas Dynamic Charts for Equilibrium Air. TR-60-0000-09093, Space Technology Lab., Inc., April 14, 1960.

14. Fenter, F. W.: The Thermodynamic Properties of High Temperature Air. Rep. RE-1R-14, Chance Vought Research Center, June 28, 1961.

15. Moeckel, W. E., and Weston, K. C.: Composition and Thermodynamic Properties of Air in Chemical Equilibrium. NASA TN 4265, 1958.

16. Kivel, B., and Bailey, K.: Tables of Radiation From High Temperature Air. Rep. 21, AVCO Res. Lab., Dec. 1957.

17. Meyerott, R. E., Sokoloff, J., and Nicholls, R. W.: Absorption Coefficients of Air. LMSD 288052, Lockheed Aircraft Corp., July 1960.

18. Camm, J. C., Kivel, B., Taylor, R. L., and Teare, J. D.: Absolute Intensity of Non-equilibrium Radiation in Air and Stagnation Heating at High Altitude. Res. Rep. 93, AVCO Res. Lab., Dec. 1959.

19. Placzek, G.: The Functions $E_n(x) = \int_1^\infty e^{-xu} u^{-n} du$. Rep. MT 1, Nat'l Res. Council of Canada. Div. of Atomic Energy, Dec. 2, 1946.

20. LeCaine, J.: A Table of Integrals Involving the Functions $E_n(x) - \int_1^\infty e^{-xu} u^{-n} du$. Rep. MT 131, Nat'l Res. Council of Canada, 1960.

21. Hansen, C. F.: Approximations for the Thermodynamic and Transport Properties of High-Temperature Air. NACA TN 4150, 1958.

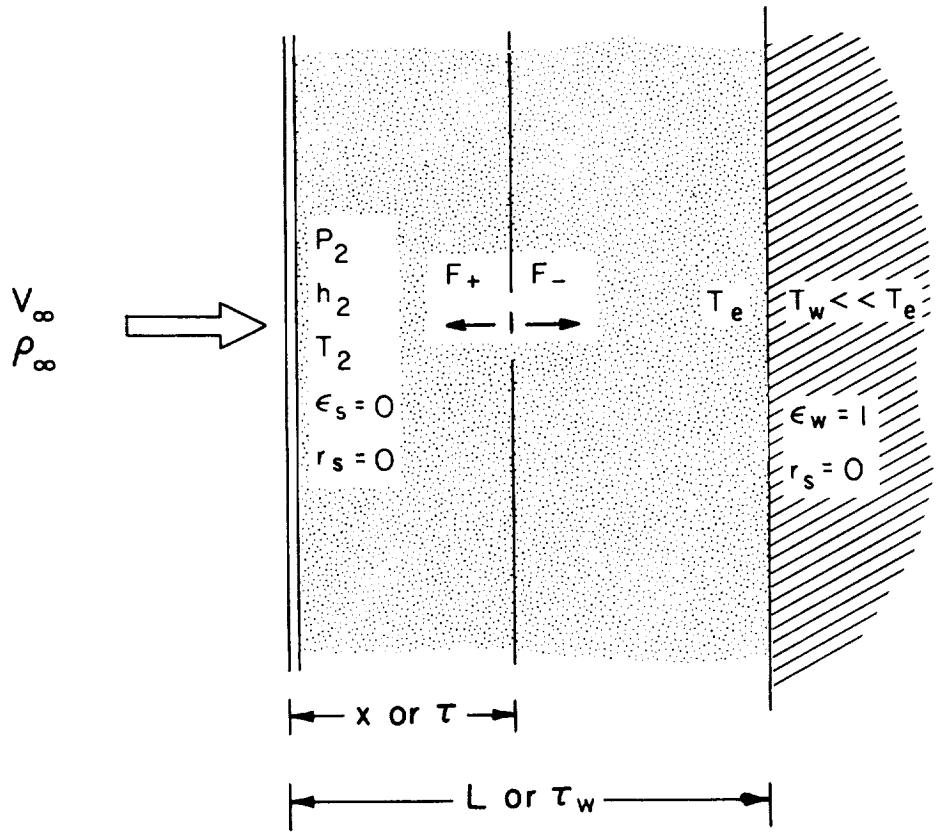

Figure 1.- Schematic diagram of radiation region behind normal shock wave.

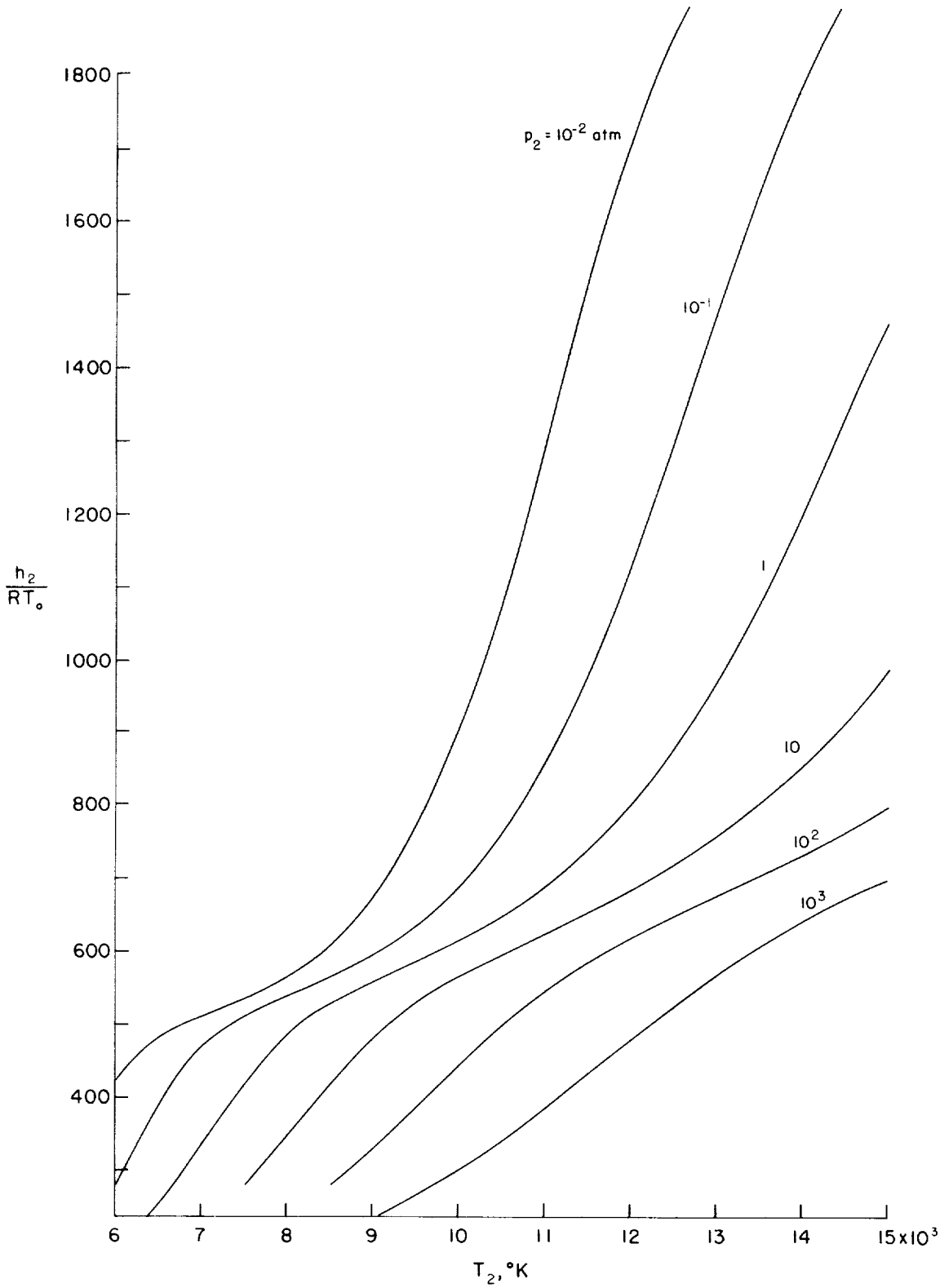

Figure 2.- Enthalpy of air at constant pressure.

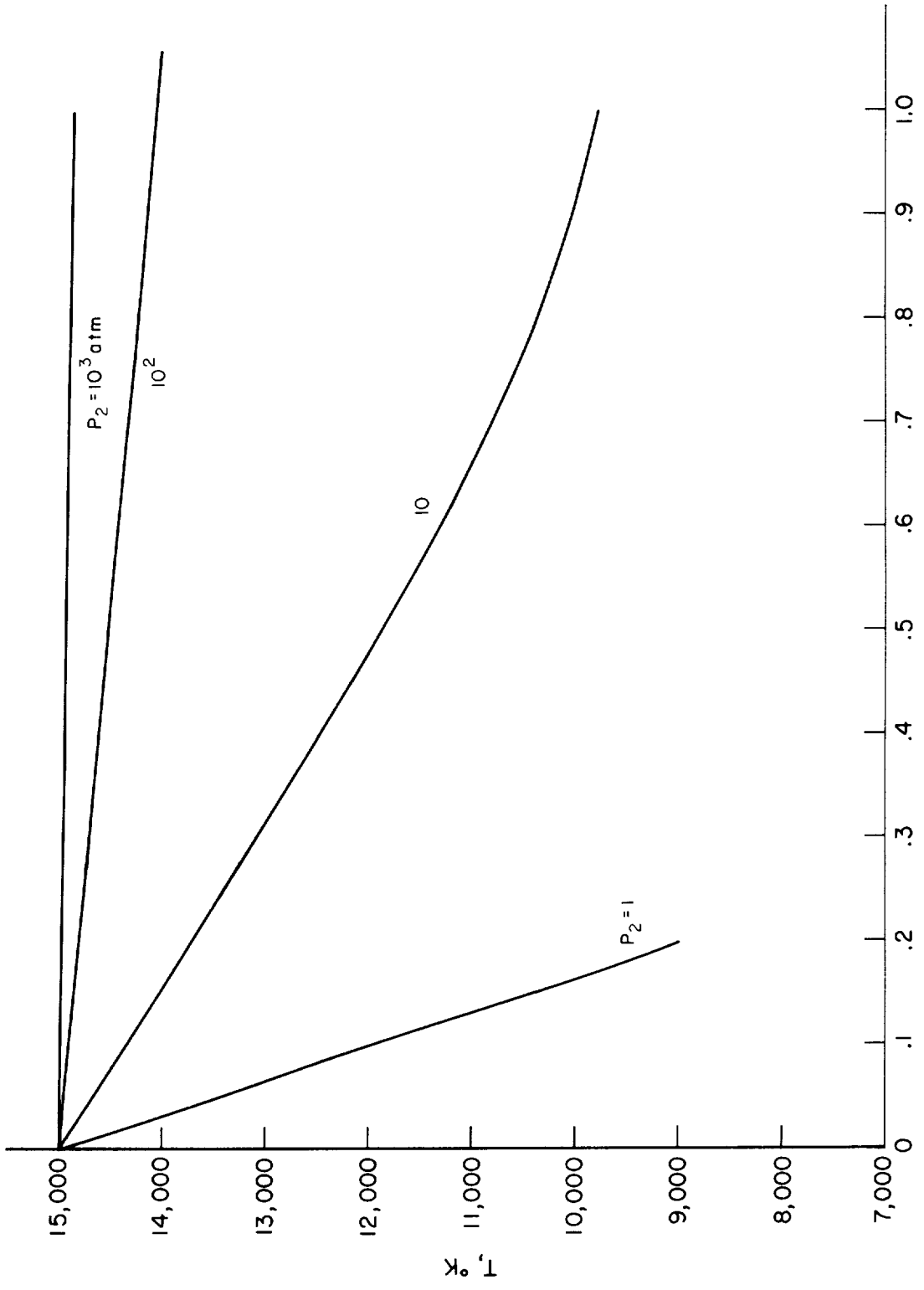

Figure 3.- Temperature as a function of F_1.

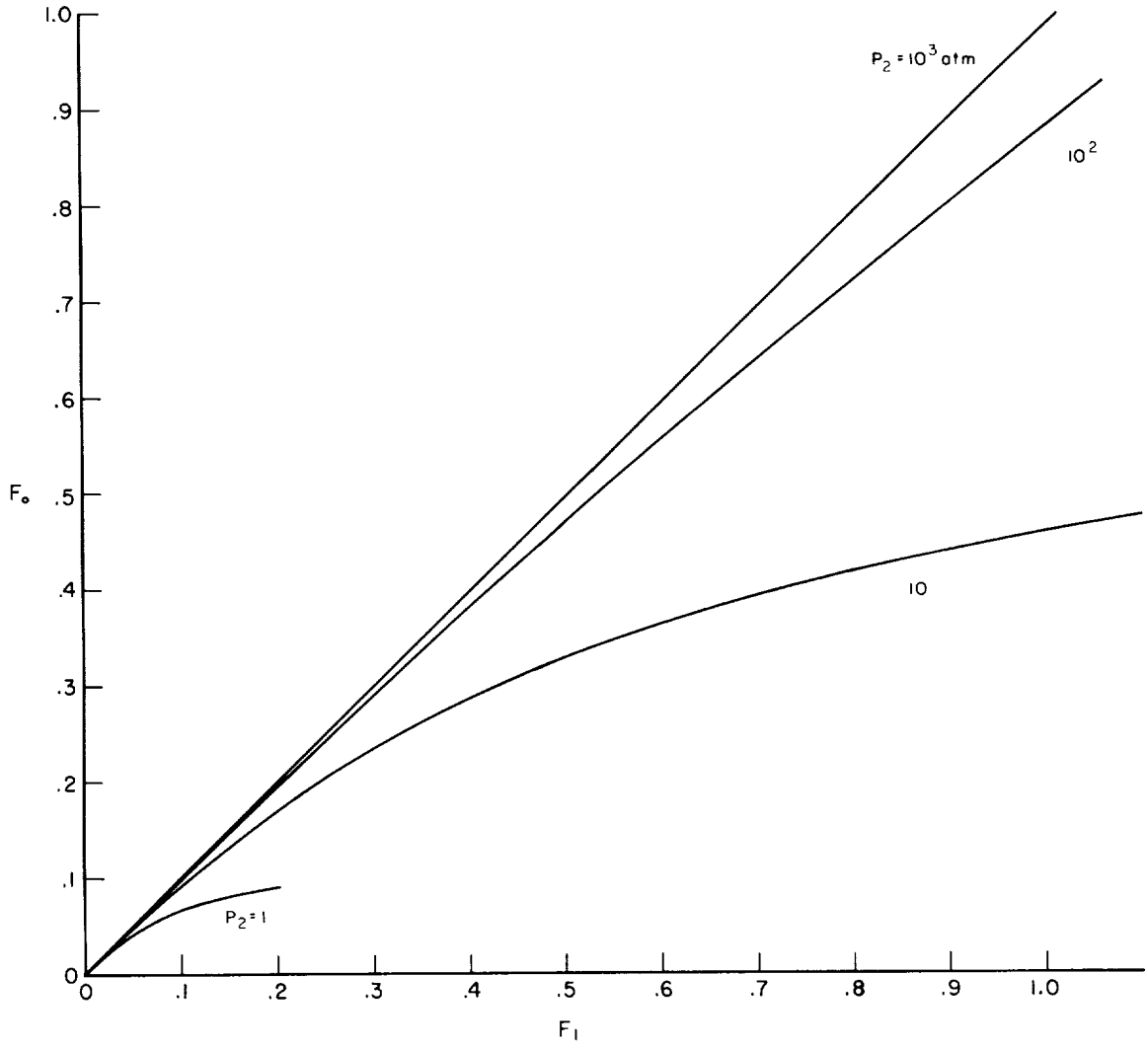

Figure 4.- F_O as a function of F_1.

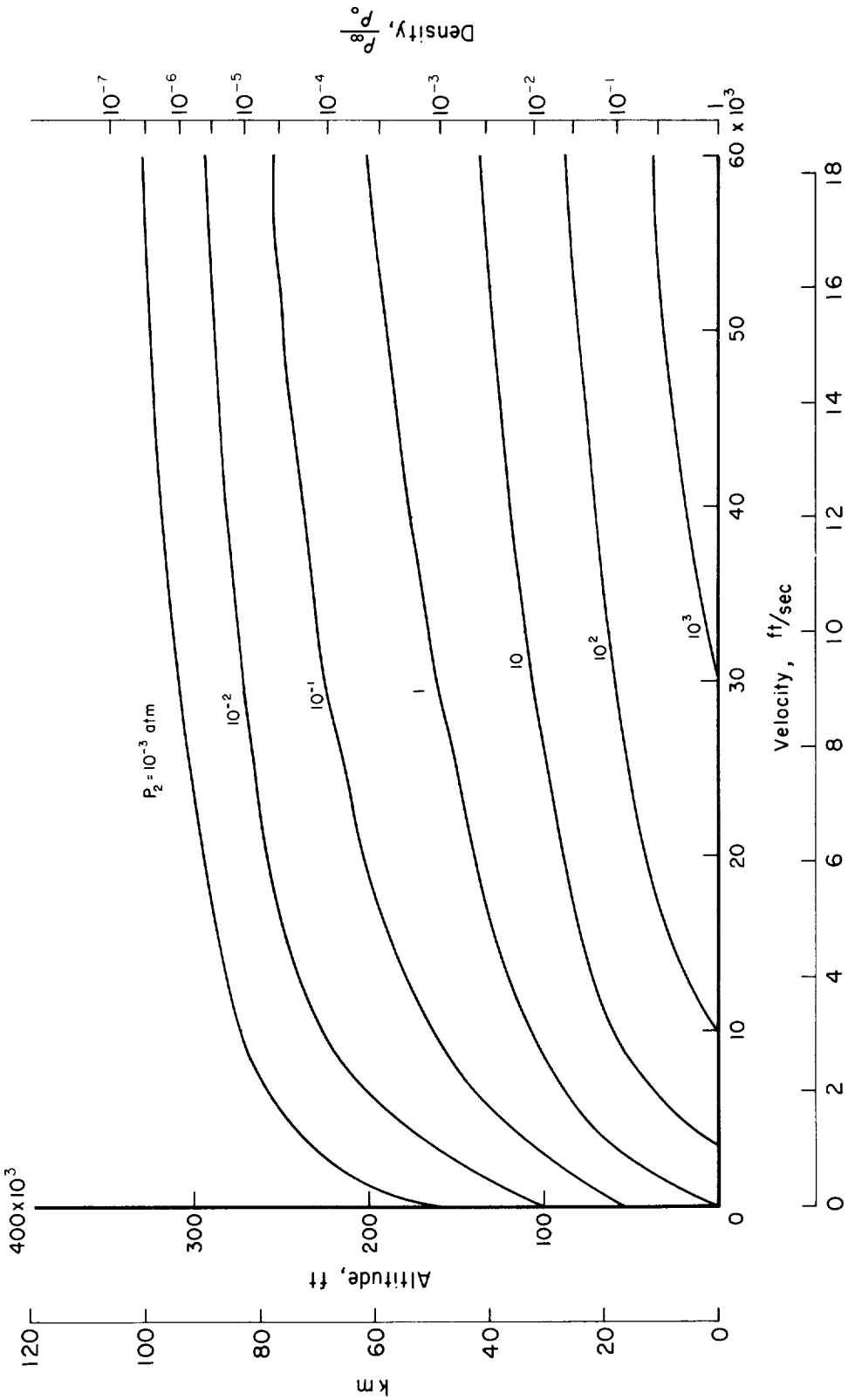

Figure 5.- Pressure behind normal shock wave.

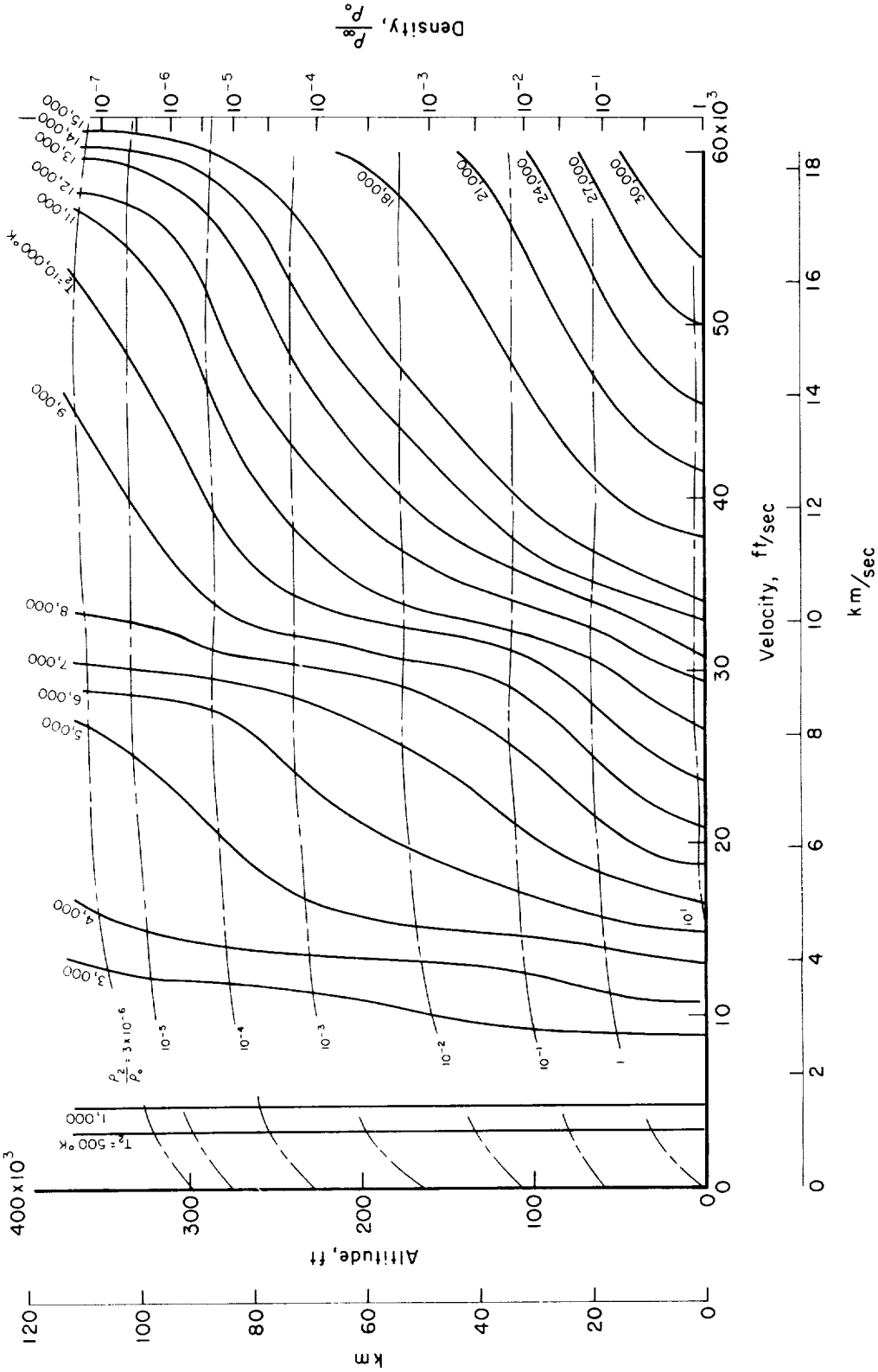

Figure 6.- Temperature and density behind normal shock wave.

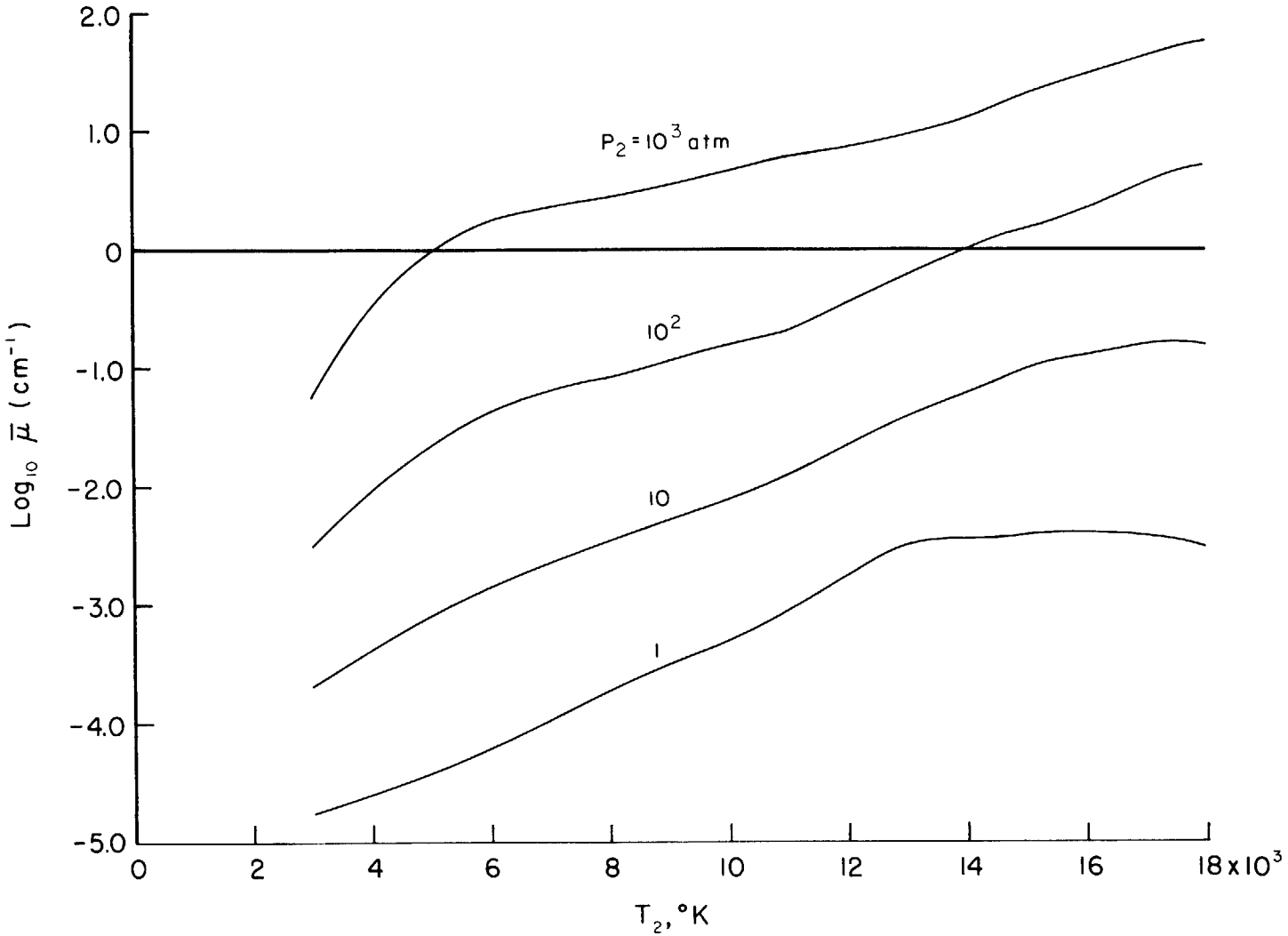

Figure 7.- Planck mean absorption coefficient (air).

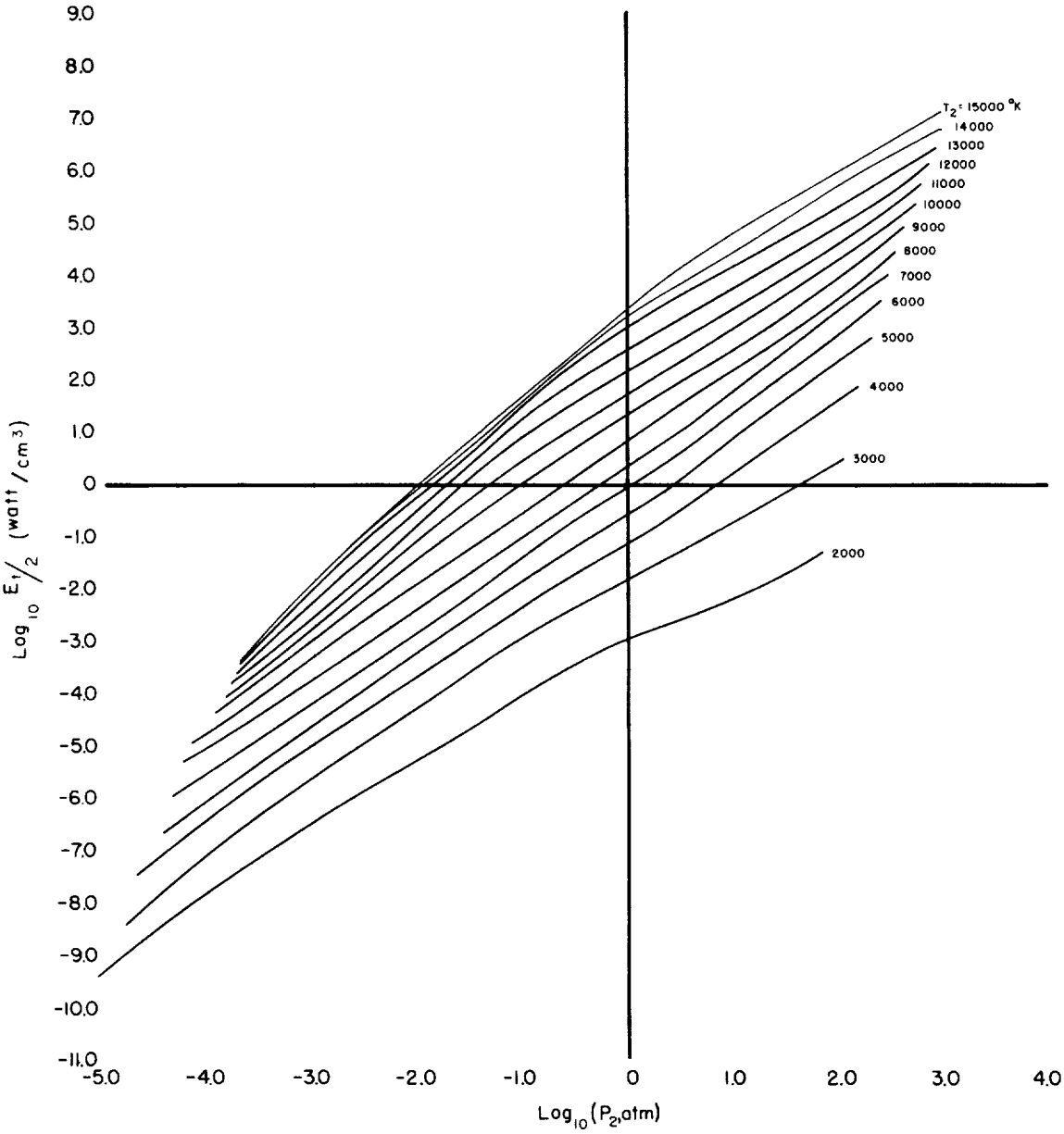

Figure 8.- Total radiation intensity (one direction).

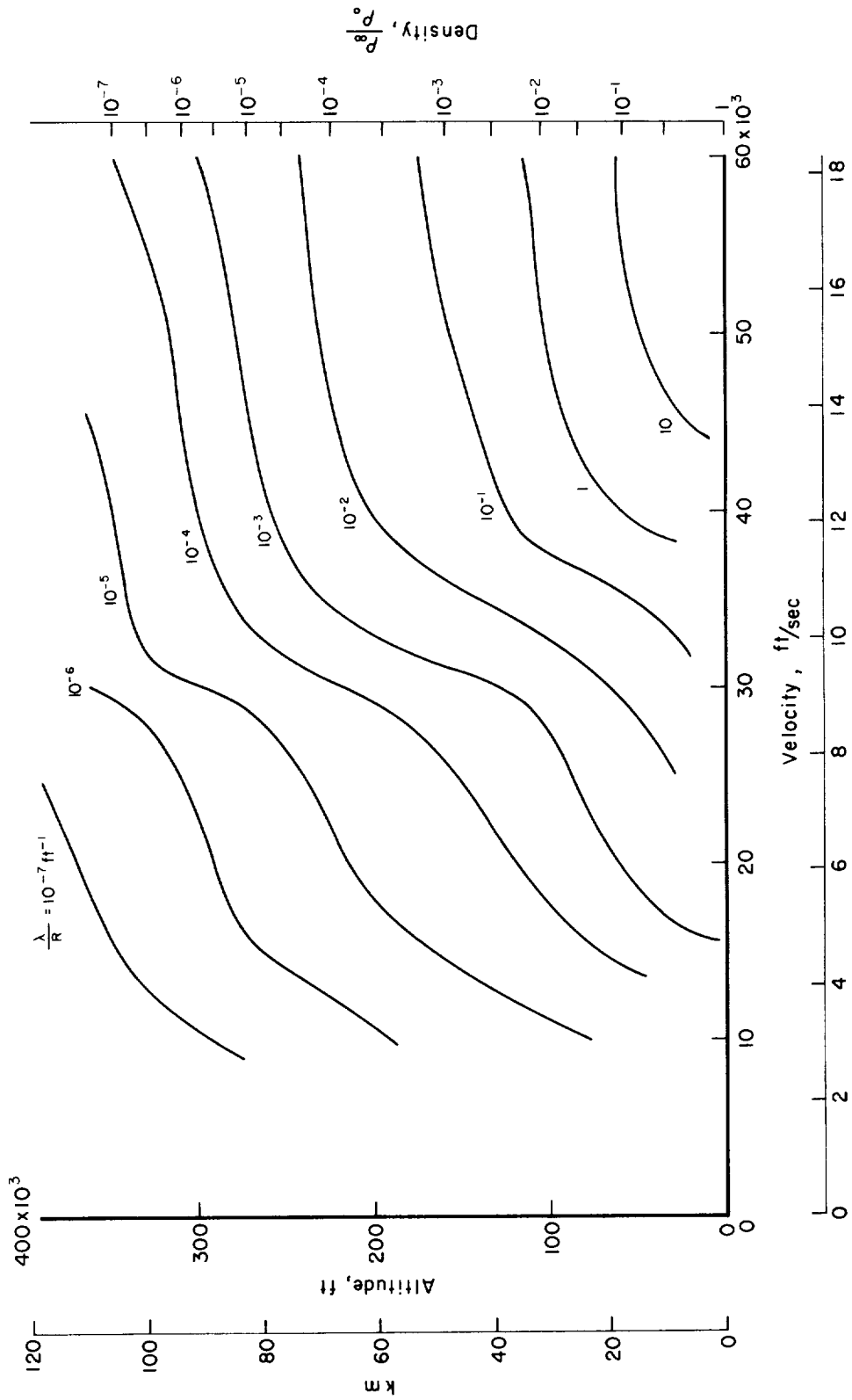

Figure 9.- Radiative heat-transfer rate at stagnation point for no absorption or decay.

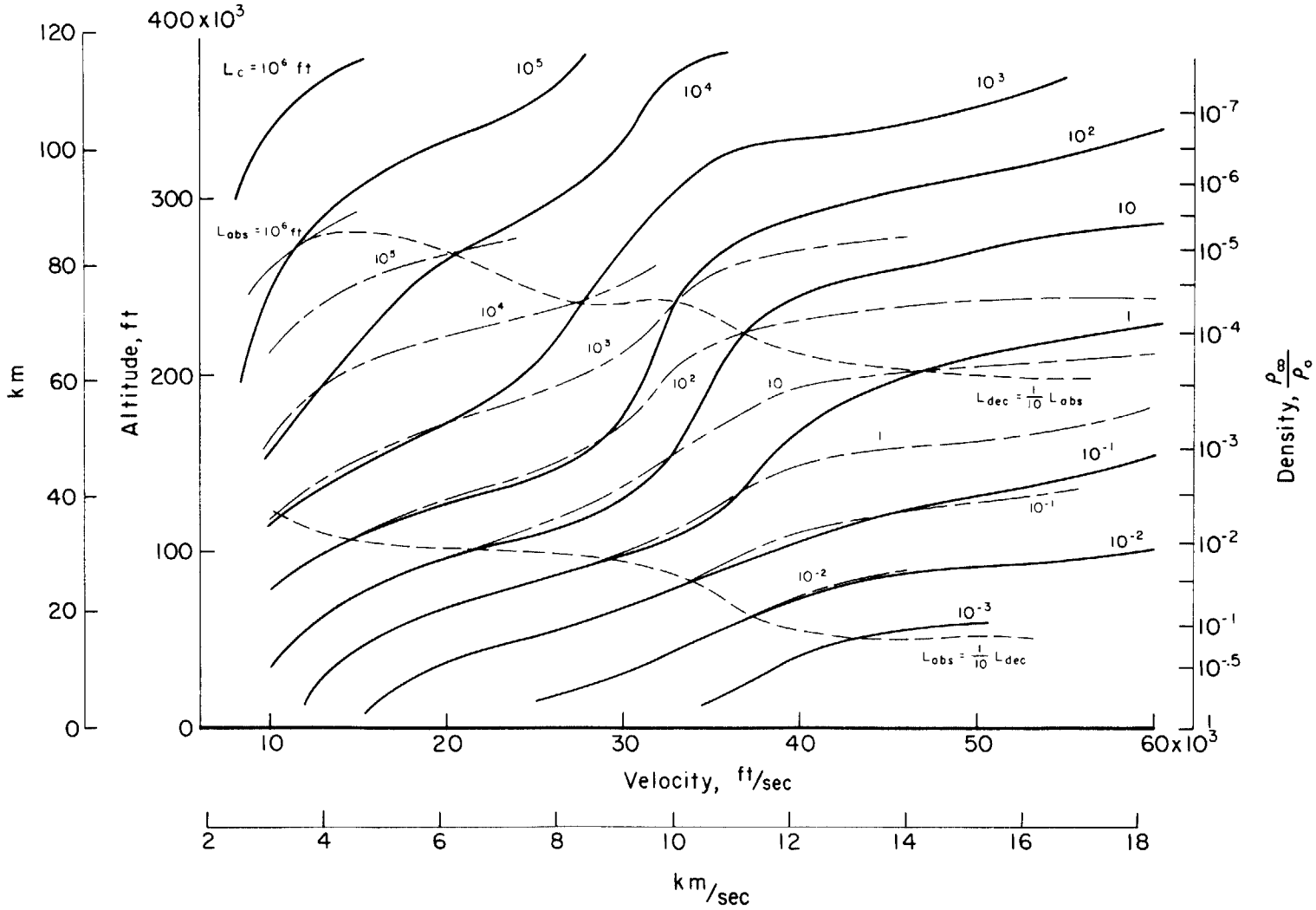

Figure 10.- Characteristic length.

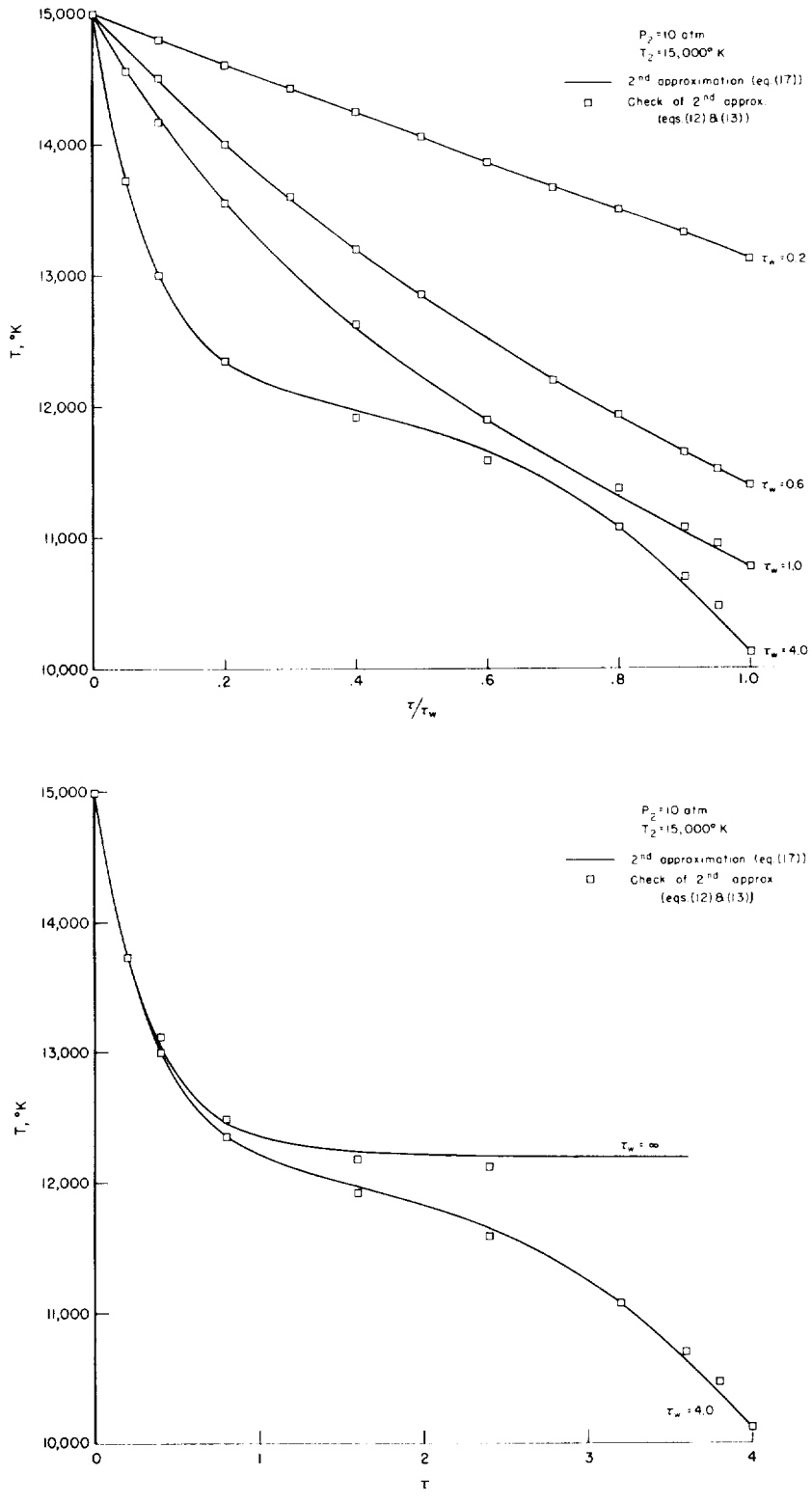

Figure 11.- Temperature distribution as a function of optical thickness.

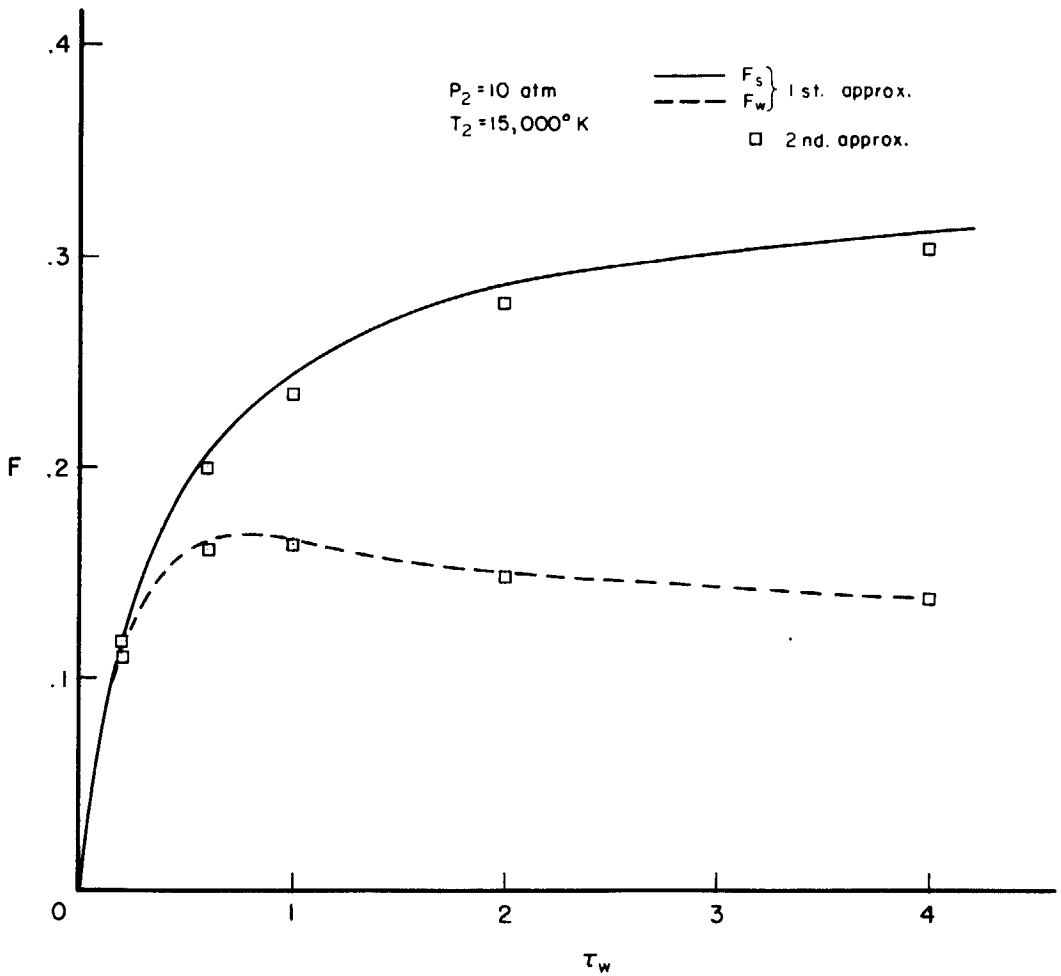

Figure 12.- First and second approximations for radiation flux as a function of optical thickness.

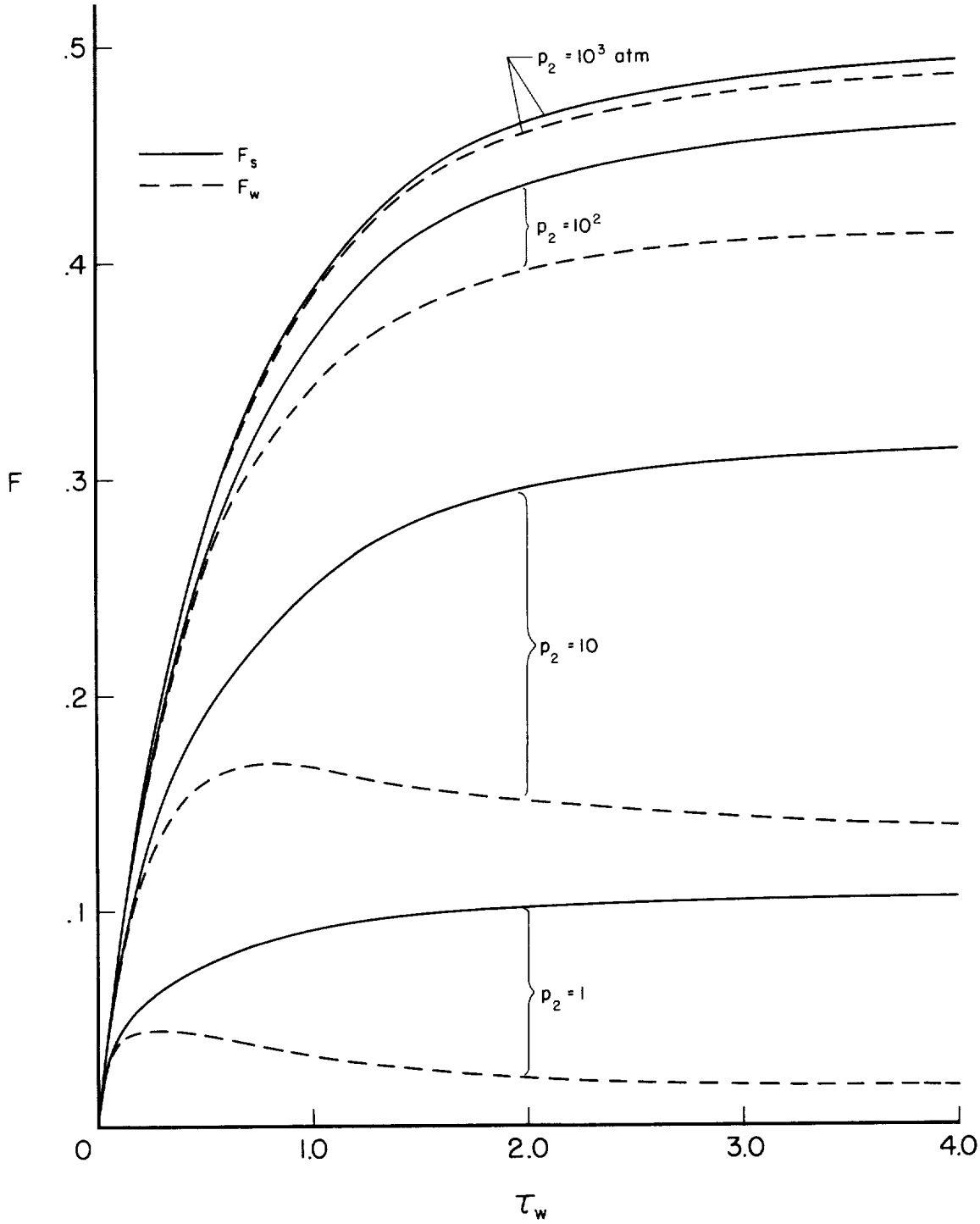

(a) $T_2 = 15{,}000^\circ$ K

Figure 13.- Radiation flux as a function of optical thickness.

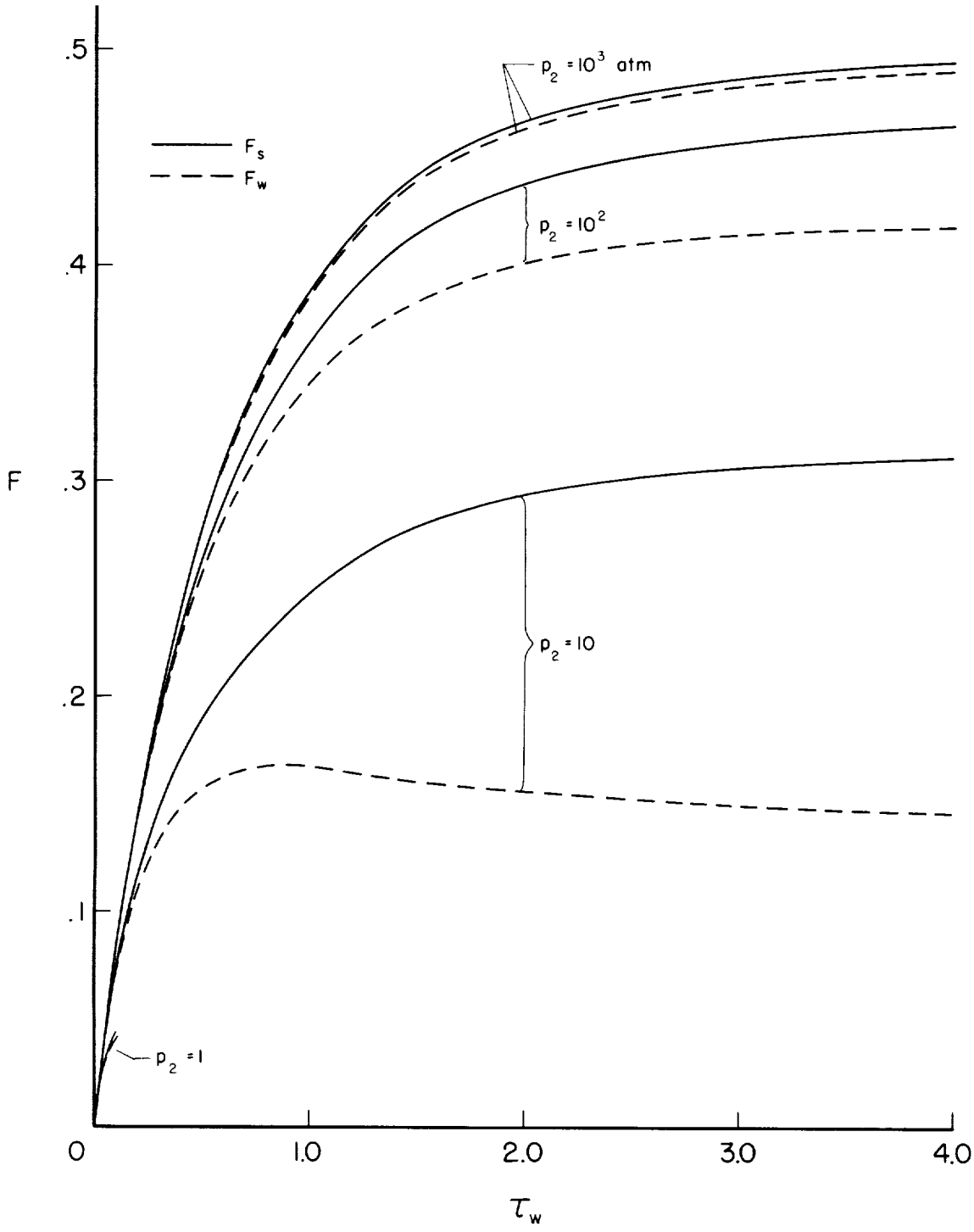

(b) $T_2 = 14{,}000^\circ$ K

Figure 13.- Continued.

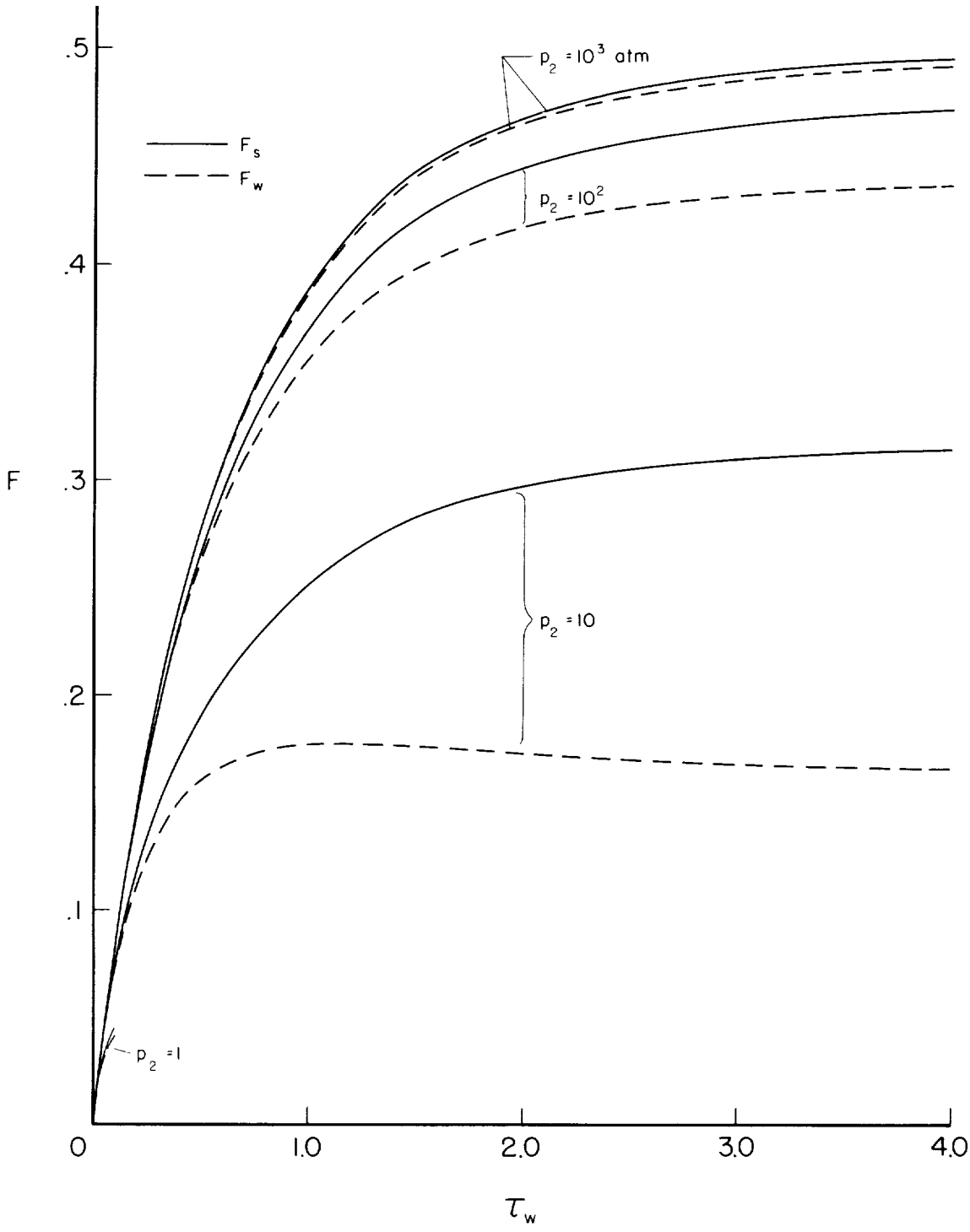

(c) $T_2 = 13{,}000^\circ$ K

Figure 13.- Continued.

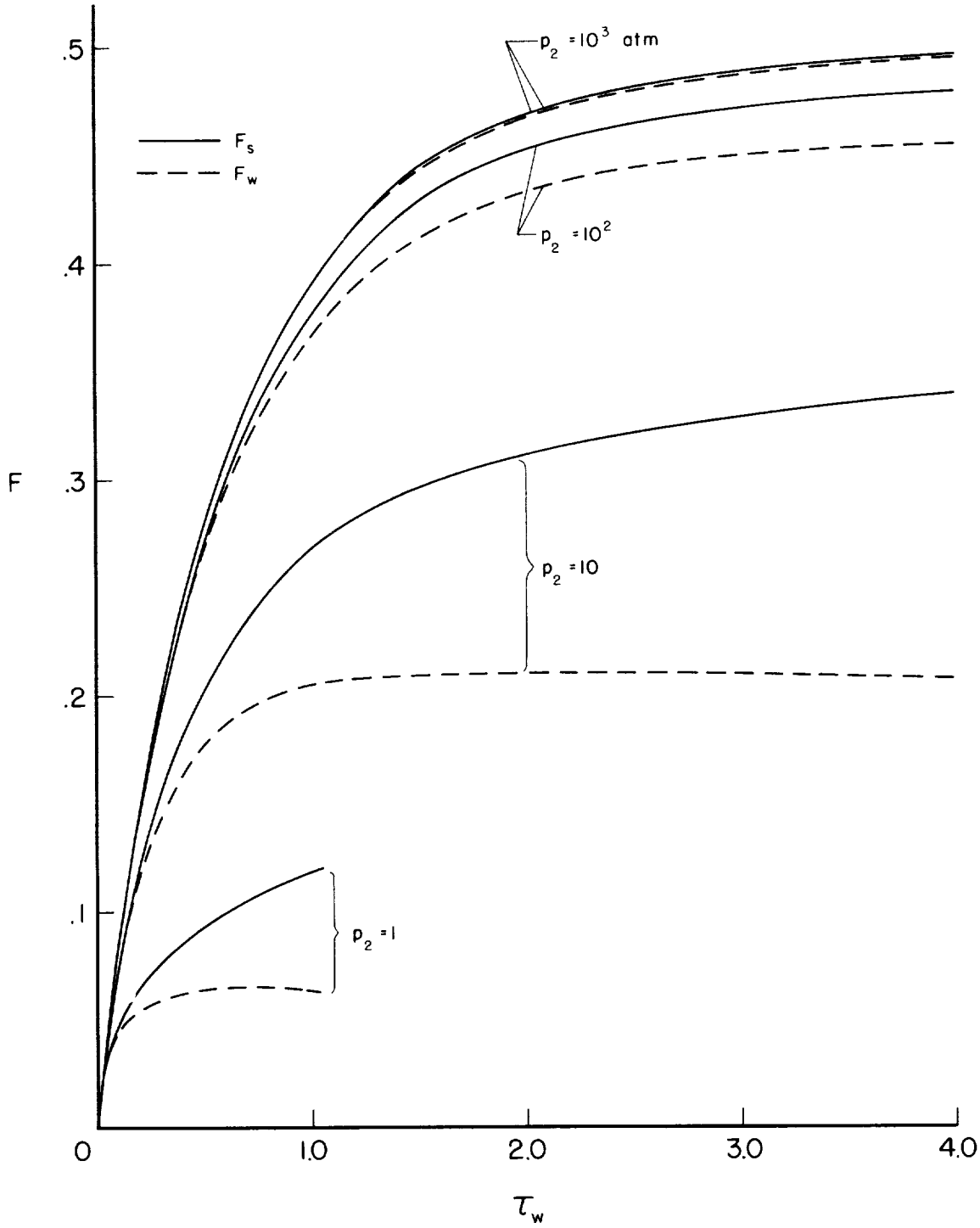

(d) T_2 = 12,000° K

Figure 13.- Continued.

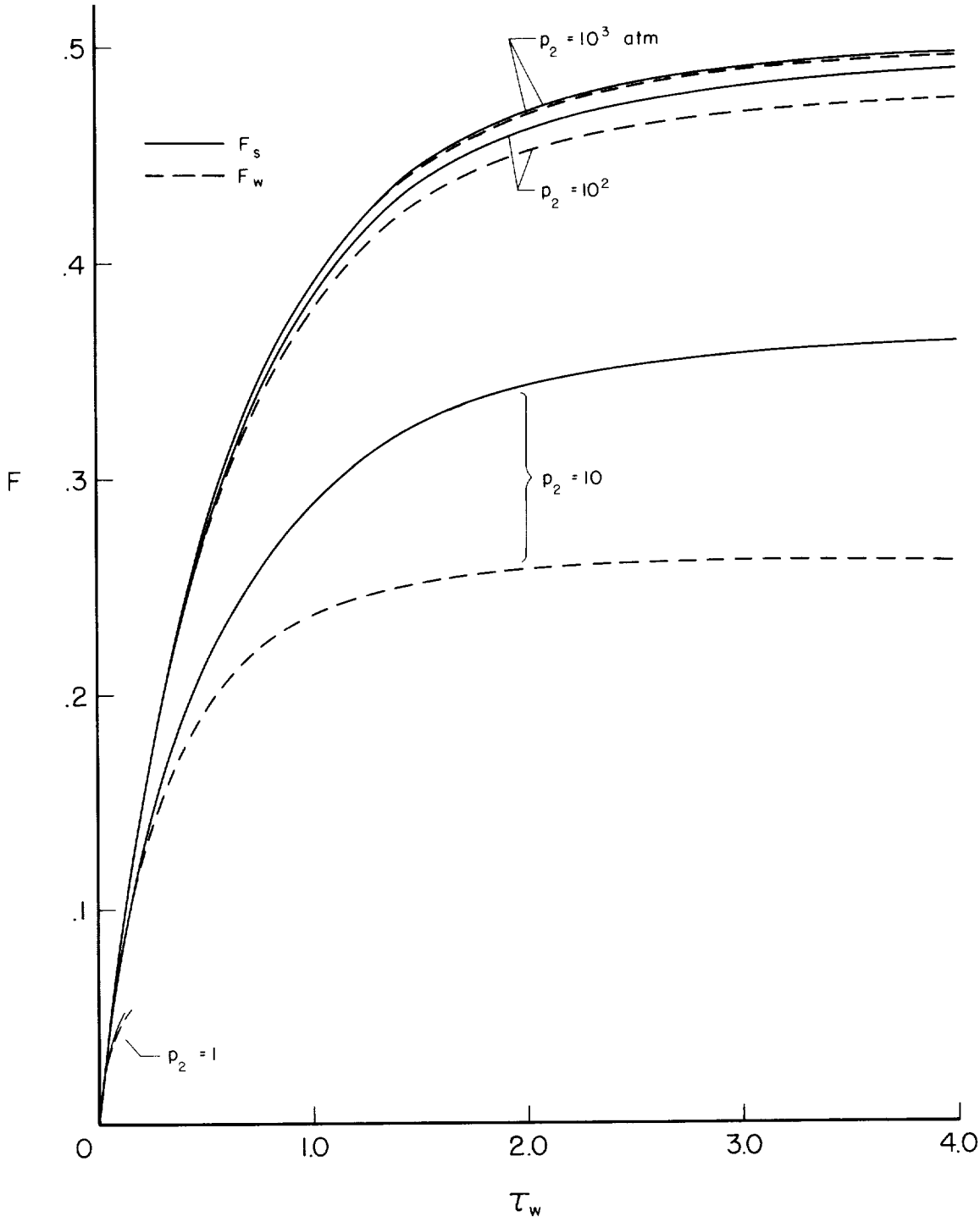

(e) $T_2 = 11{,}000^\circ$ K

Figure 13.- Continued.

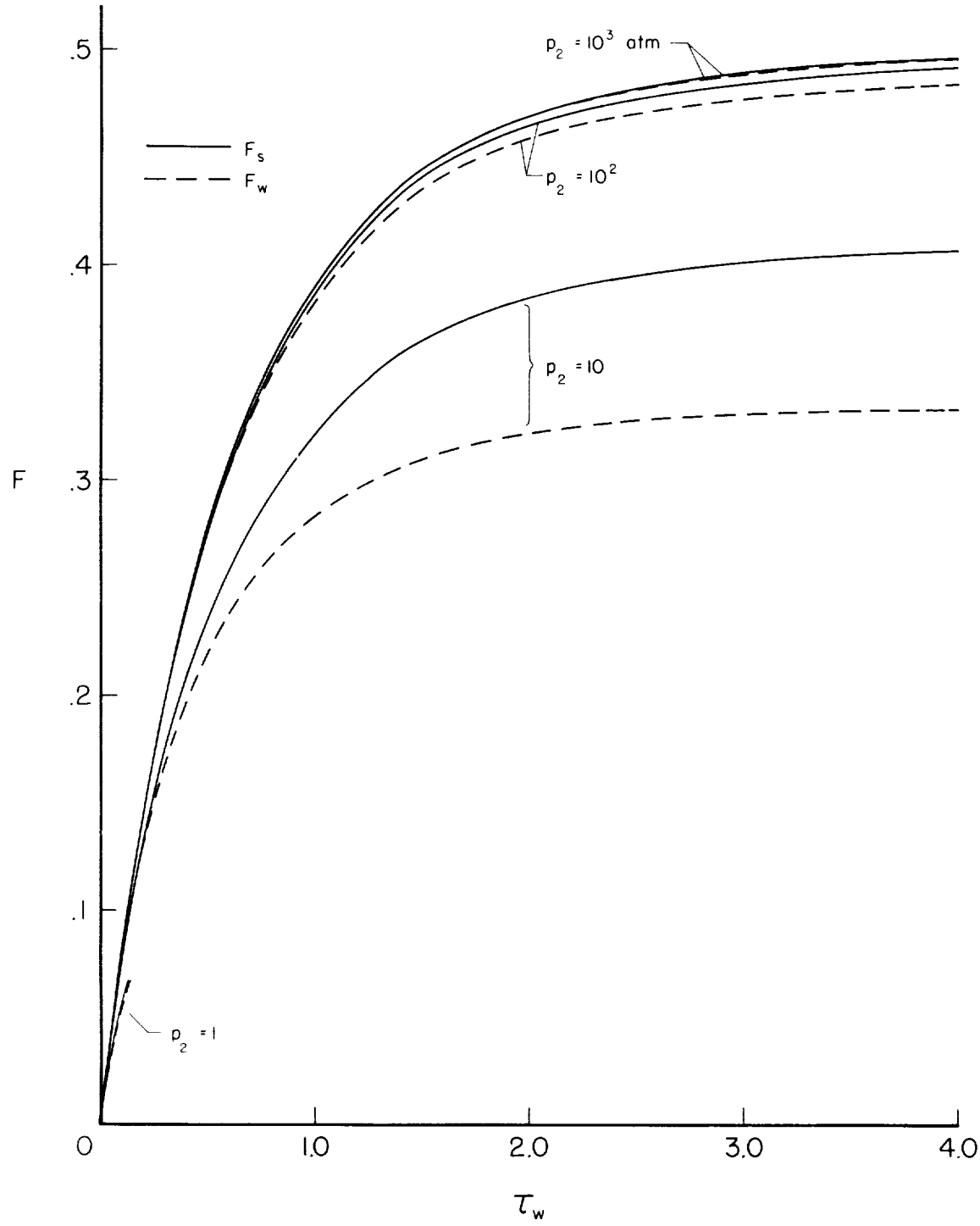

(f) T_2 = 10,000° K

Figure 13.- Concluded.

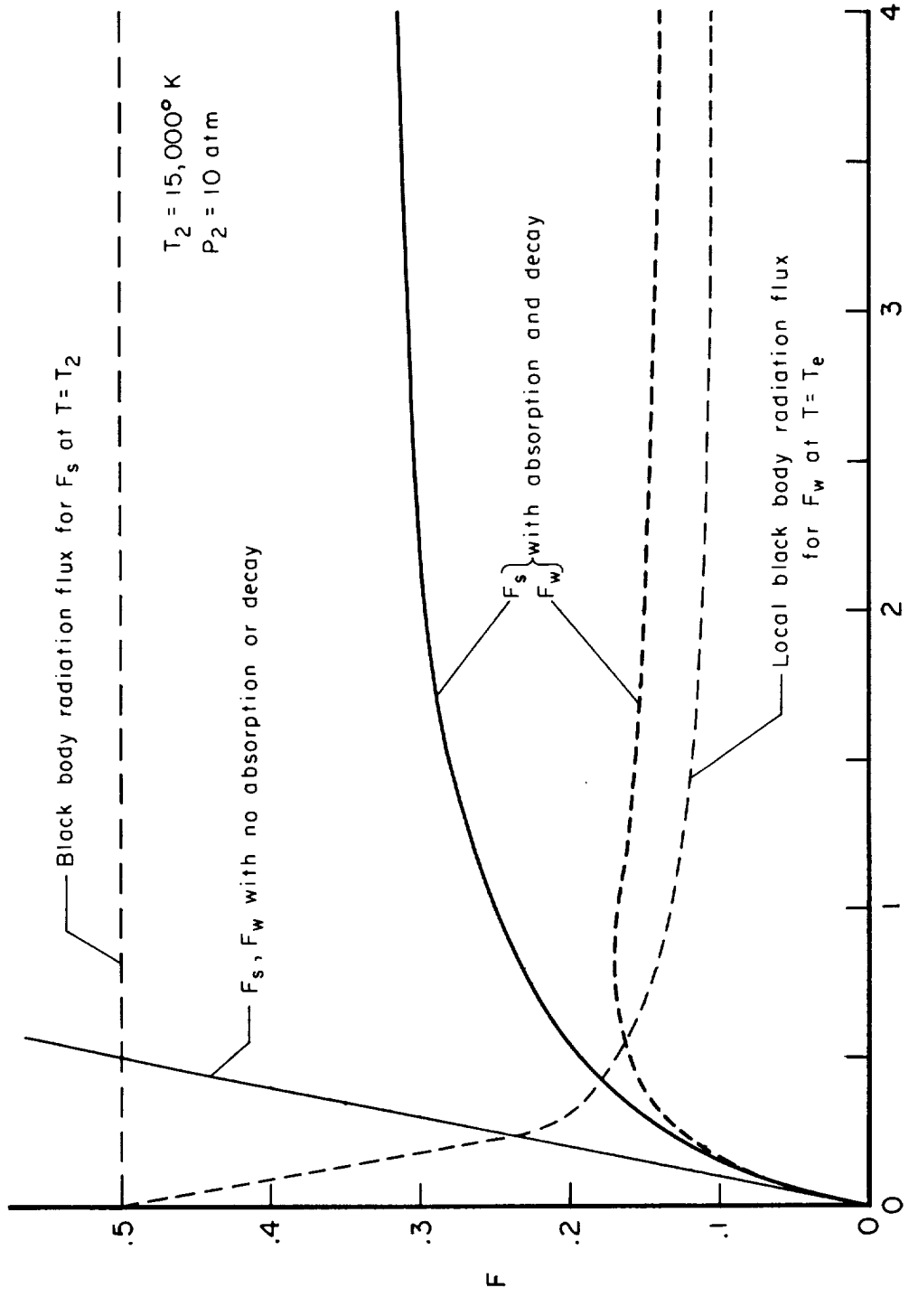

Figure 14.- Comparison of radiation flux with absorption and decay to radiation flux without absorption and decay.

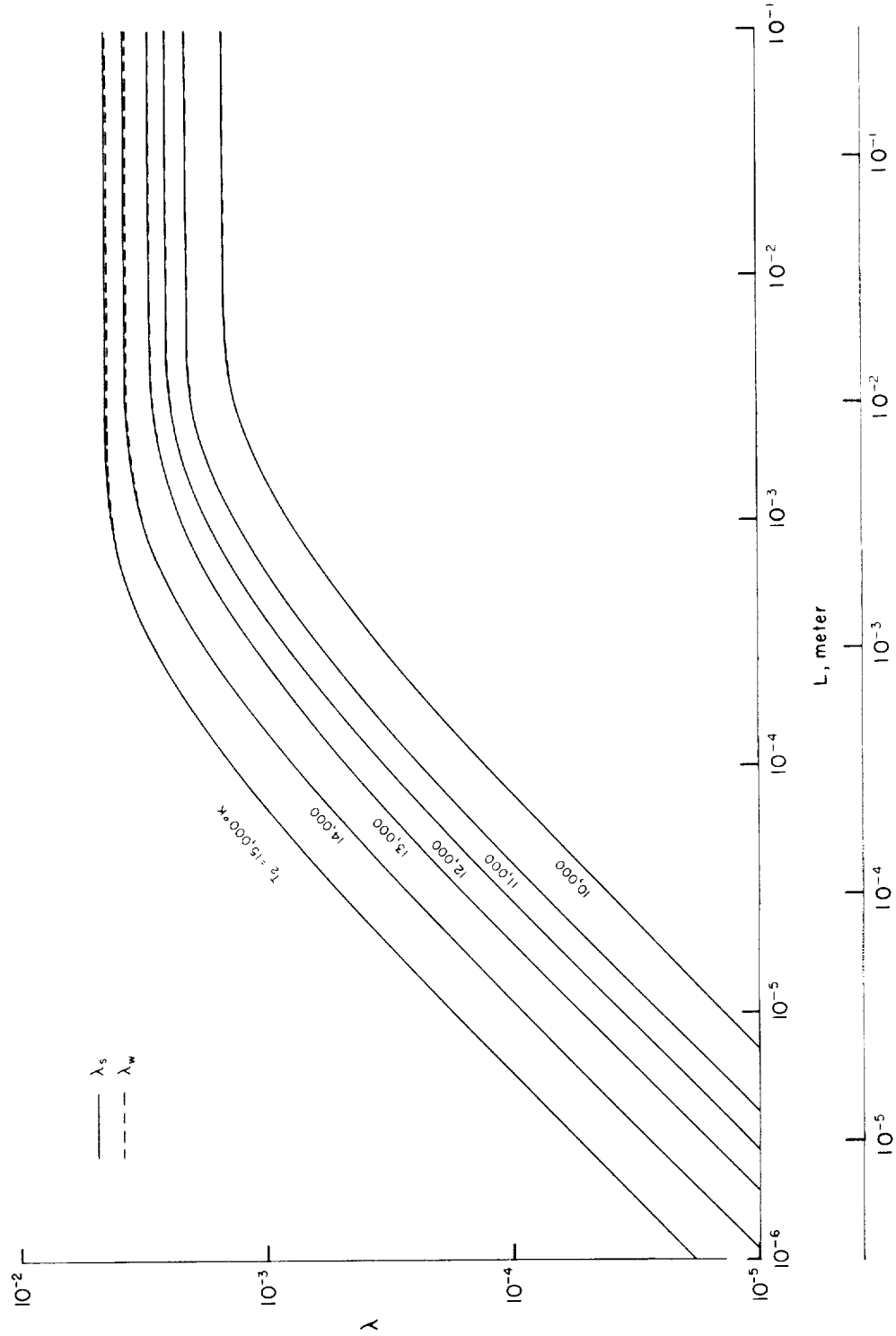

(a) $p_2 = 10^3$ atm

Figure 15.- Radiative heat-transfer coefficient as a function of shock standoff distance.

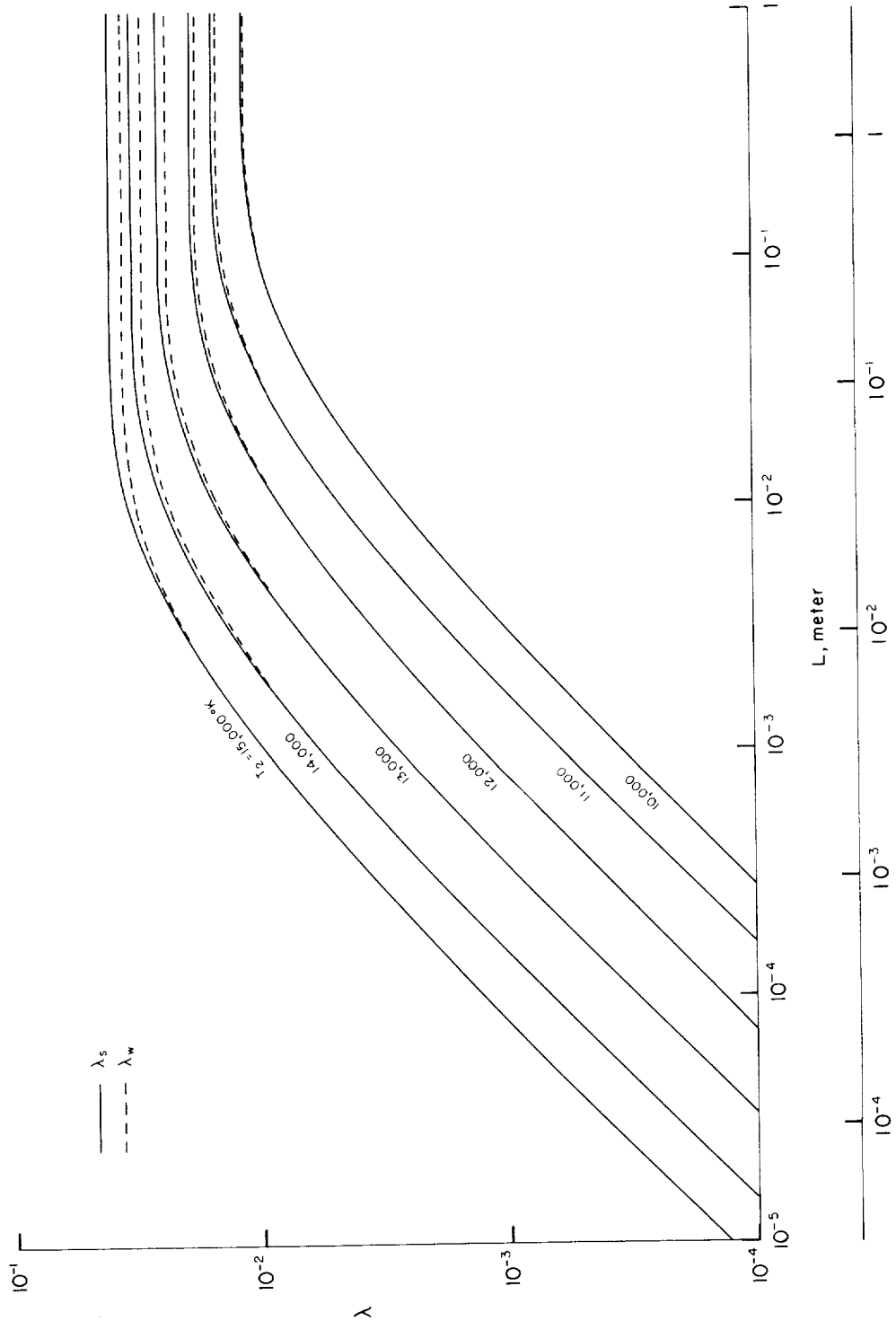

(b) $p_2 = 10^2$ atm

Figure 15.- Continued.

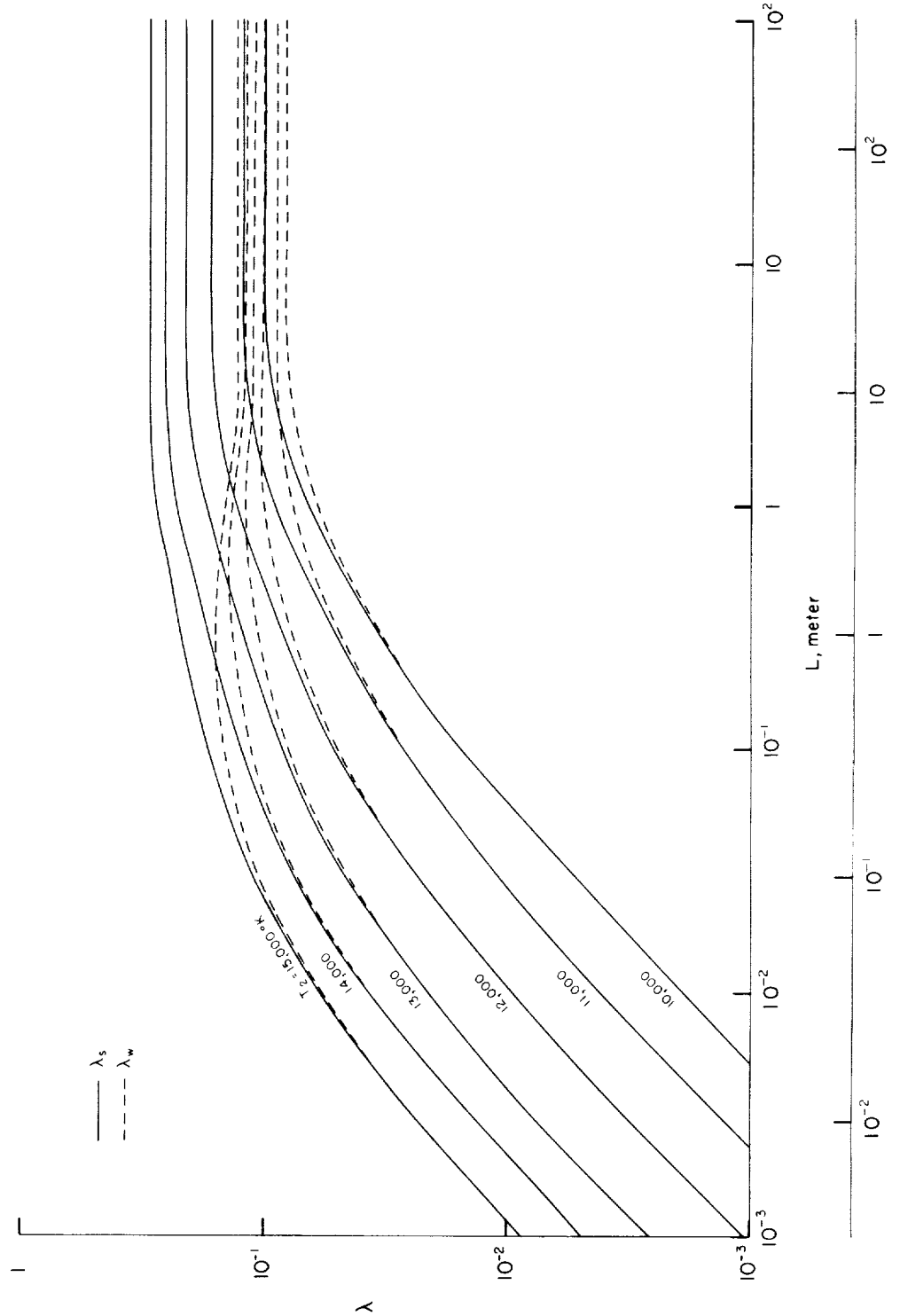

(c) p_2 = 10 atm

Figure 15.- Continued.

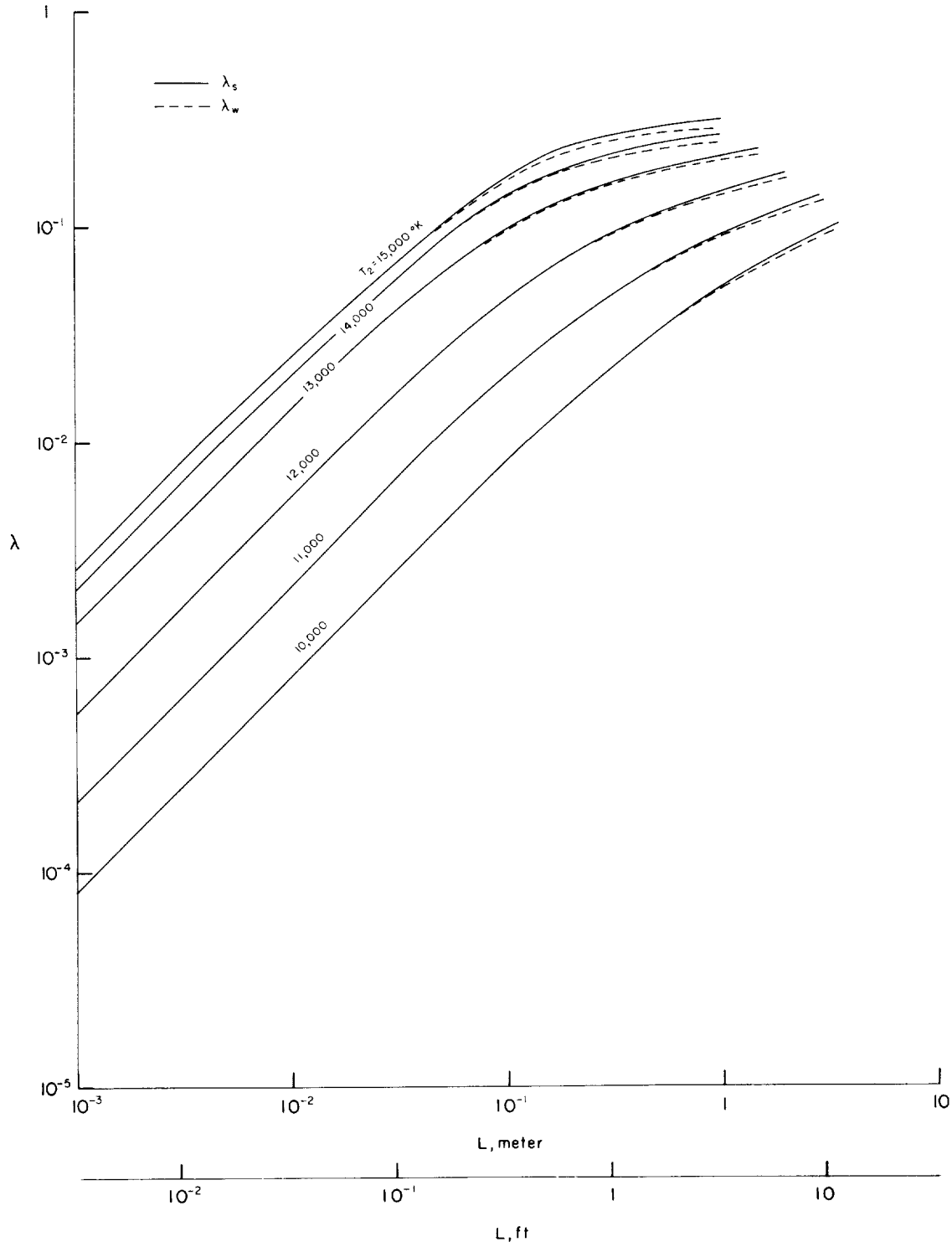

(d) p_2 = 1 atm

Figure 15.- Concluded.

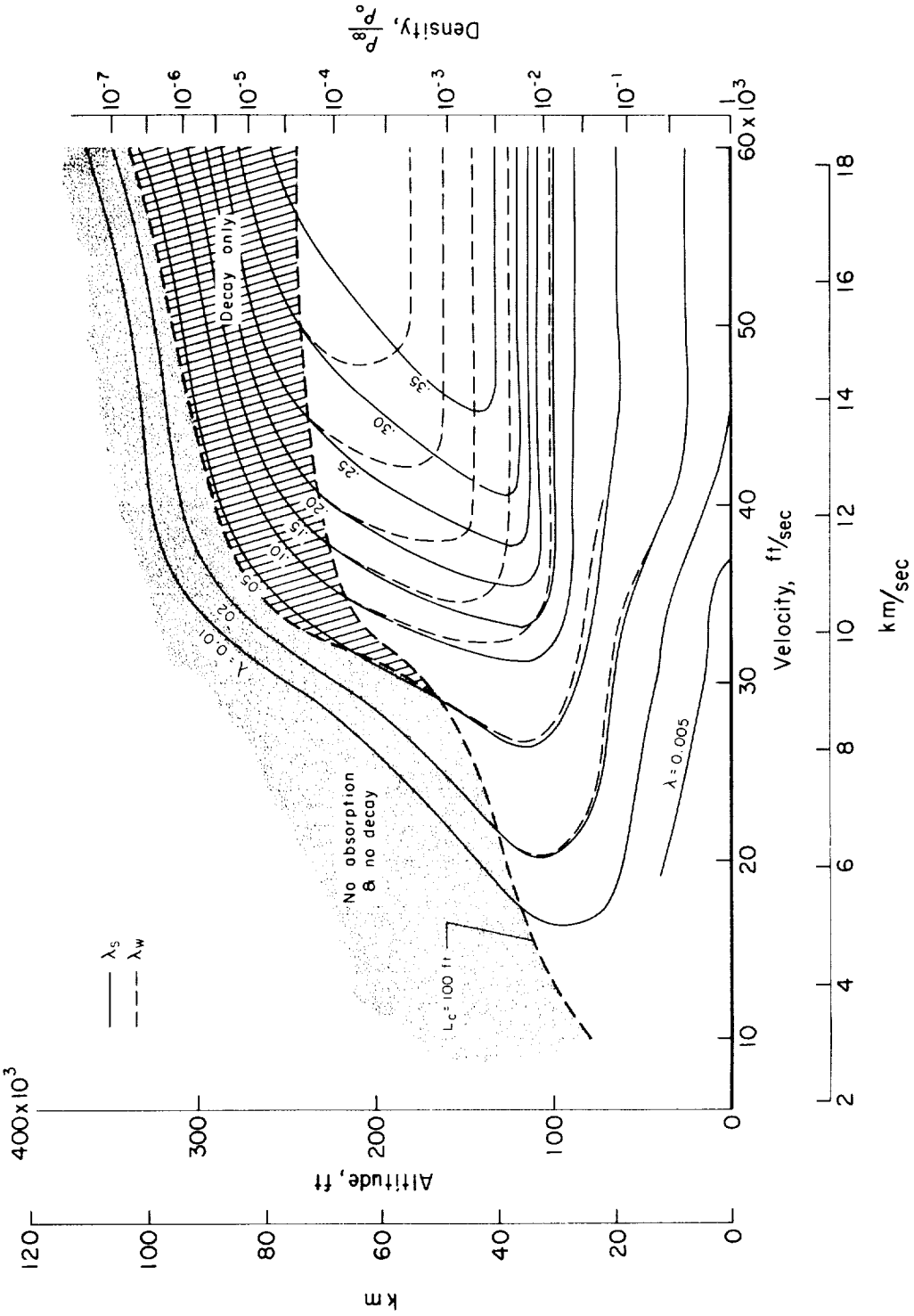

(a) L = 10 ft

Figure 16.- Radiative heat-transfer coefficient for various flight conditions.

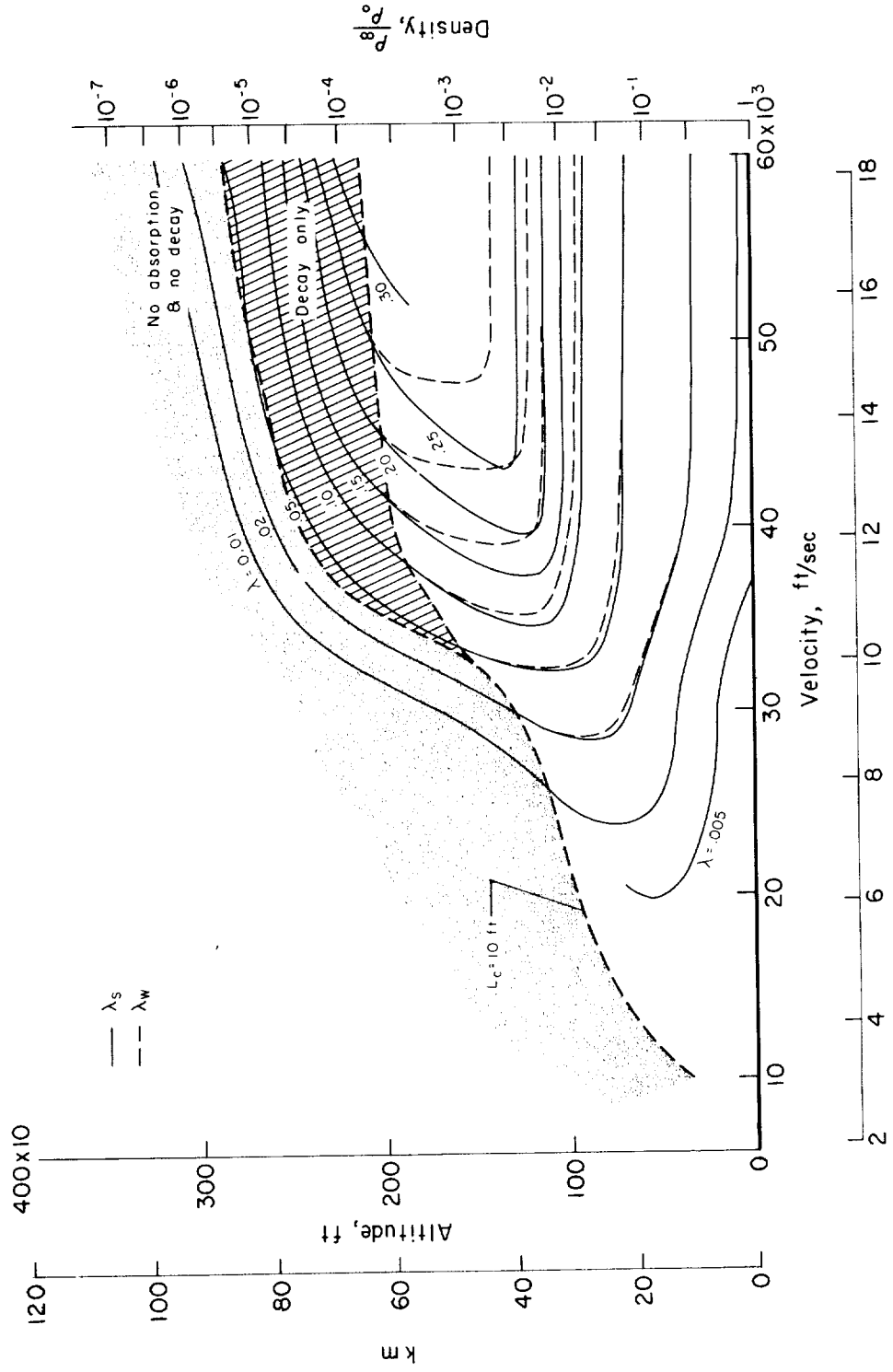

(b) L = 1 ft

Figure 16.- Continued.

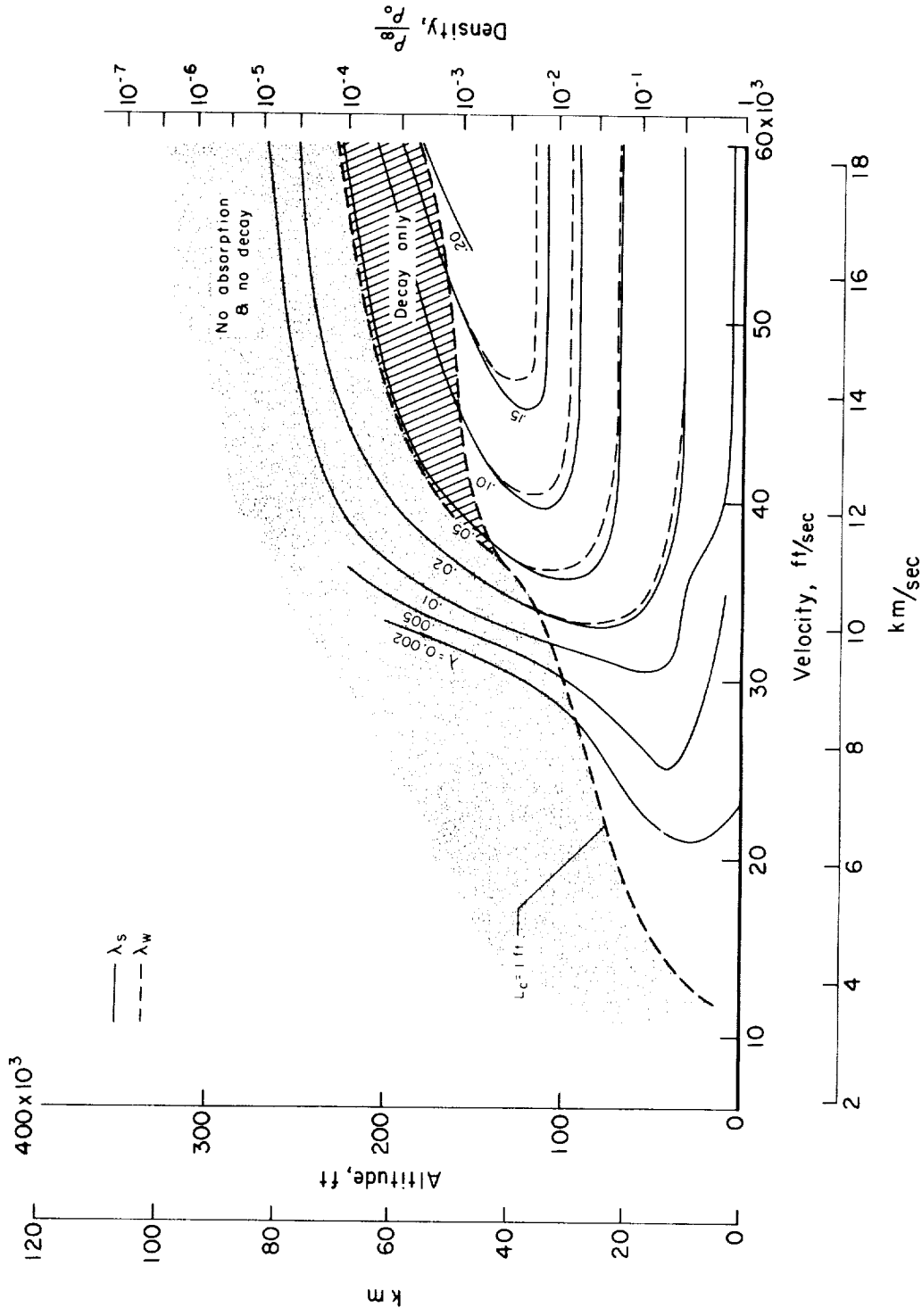

(c) L = 0.1 ft

Figure 16.- Continued.

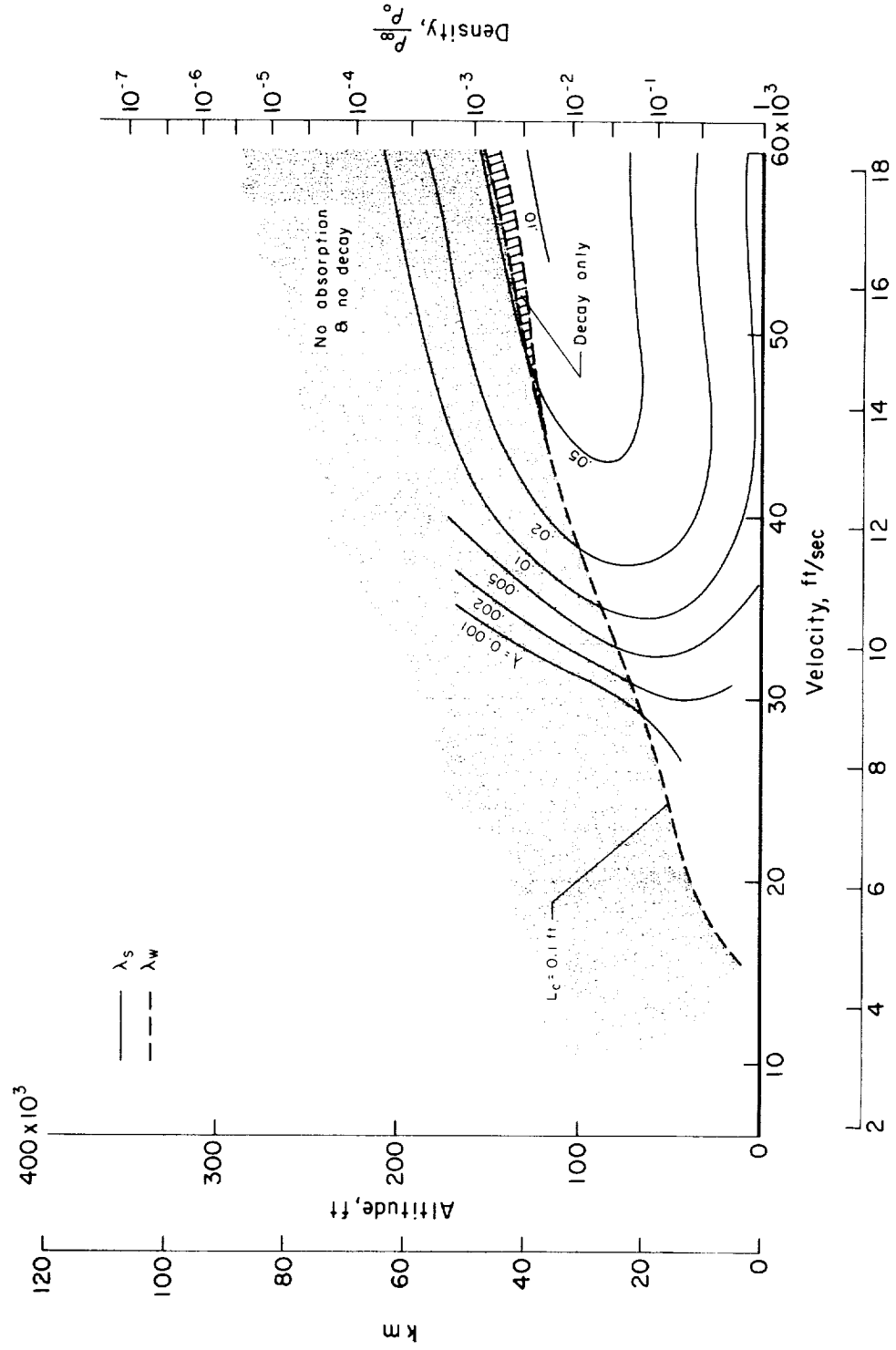

(d) L = 0.01 ft

Figure 16.- Concluded.